LA-3686-MS

LOS ALAMOS SCIENTIFIC LABORATORY
of the
University of California
LOS ALAMOS • NEW MEXICO

Quarterly Status Report on the Advanced Plutonium Fuels Program January 1 - March 31, 1967

UNITED STATES
ATOMIC ENERGY COMMISSION
CONTRACT W-7405-ENG. 36

DISCLAIMER

LEGAL NOTICE

This LA...MS report presents the status of the LASL Advanced Plutonium Fuels program. Previous quarterly status reports in this series, all unclassified, are:

LA-3607-MS
LA-3650-MS

This report, like other special-purpose documents in the LA...MS series, has not been reviewed or verified for accuracy in the interest of prompt distribution.

Printed in the United States of America. Available from Clearinghouse for Federal Scientific and Technical Information National Bureau of Standards, U. S. Department of Commerce Springfield, Virginia 22151
Price: Printed Copy $3.00; Microfiche $0.65

LA-3686-MS
SPECIAL DISTRIBUTION

LOS ALAMOS SCIENTIFIC LABORATORY
of the
University of California
LOS ALAMOS • NEW MEXICO

Report distributed: April 24, 1967

Quarterly Status Report on the Advanced Plutonium Fuels Program January 1 - March 31, 1967

FOREWORD

This is the third quarterly report issued on work in the Advanced Plutonium Fuels Program at the Los Alamos Scientific Laboratory. The results described may be of a preliminary nature; no published reference of these preliminary results or quotation of them should be made without explicit permission from the persons in charge of the work.

PROJECT 801

RELEASE, DISTRIBUTION, AND REMOVAL OF FISSION PRODUCTS IN SODIUM COOLANT SYSTEMS

Person in Charge: D. B. Hall
Principal Investigators: R. H. Perkins
J. C. Clifford

I. INTRODUCTION

The behavior of fission products released to sodium coolant from failed or deliberately vented reactor fuel elements may limit access to the primary coolant system, affect the consequences of a loss-of-coolant incident, and influence the compatibility of materials. Depending on the fission-product inventory resulting in the primary coolant system, it may be desirable to concentrate uranium, plutonium, long-lived energetic gamma-emitting isotopes, and short-lived biologically hazardous isotopes at specific locations within the system. To this end the interaction of plutonium-based fuels with sodium is being investigated. The study includes the release and distribution of fission products from irradiated fuel to sodium, and methods by which the distribution may be altered.

Two types of laboratory experiments are being used: encapsulation of sodium with irradiated fuel or a single radioisotope in small tubes; and contact of irradiated fuel and sodium in small, forced-convection sodium loops. In both types of experiment, *in situ* gamma-ray spectrometry is the principal analytical tool, augmented by wet radiochemical analyses.

The release of fission products to sodium from trace-irradiated fuel is studied with capsules. The loop experiments determine the general distribution of fission products in a sodium system together with the relative effectiveness of trapping techniques on this distribution. Trapping techniques that show merit are also examined in further capsule experiments, using a single radioisotope as the source of activity and one adsorbing material as a sink.

II. IRRADIATED FUEL - SODIUM INTERACTION STUDIES (J. C. Biery)

A. General

When nuclear reactor fuel elements containing ceramic Pu-U pellets rupture, fission products will be leached from the pellets by the sodium coolant. The release rates of these fission products should be known to evaluate sodium system contamination problems. This research program is designed to determine fission product mass transfer rates from ceramic fuel pellets to sodium as a function of temperature, sodium conditions, and pellet composition.

The release of fission products into sodium from irradiated Pu-U ceramic fuel pellets is being studied by measuring gamma count rate spectra from the pellet and the sodium into which fission products have transferred. The neutron irradiated pellet is enclosed in 3 to 10 in. of sodium in a 12-in.-long capsule. The distribution of fission products as a function of time and position in the capsule is determined by gamma scanning the capsule. The rate data obtained by integrating the curve of count rate versus position produces fission-product release rates from the pellet into the sodium. The temperatures for the experiments range from 650° to 800°C. The furnace can impose either isothermal conditions or longitudinal temperature gradients up to 25°C/in.

B. Current Results

The first experimental run which was started last quarter was completed this quarter. The data

from the run are now being analyzed, and the preliminary results are reported here.

Summary of experimental conditions:

Pellet: Size: 0.28 in. diameter x 0.23 in. high

Composition: $U_{0.8}Pu_{0.2}C_{1.0}$ hyperstoichiometric with M_2C_3 phase evident by metallographic examination

Method of production: Sintering

Density: 12.2 g/cc (approximately 90% of theortical density)

Weight of Pu: 0.60 g

Irradiation: Time: 114 hr

Average flux in pellet: 7.5×10^{10} (thermal flux). (Edge to average = 2.4; center to average = 0.4)

No. of fissions: 3.45×10^{16}

No. of atoms at end of irradiation:

^{137}Cs: 2.28×10^{15}

^{131}I : 1.120×10^{15}

Sodium column length: 3.5 in.

Sodium weight: 7.1 g

Sodium oxygen concentration: 6 ± 4 ppm

Temperature program:

408 hr at 650°C plus

410 hr at 800°C plus

700 hr with temperature gradient (741°C at pellet to 690°C at gas/liquid interface 3-1/2 in. above pellet)

Complete linear scans of the capsules were taken weekly with a NaI crystal and a 0.06 in. slit. The count time at each position ranged between 10 min to 60 min. Counts were taken at intervals of 0.10 in.

The transfer was very small and as a result the scan results were inconclusive. The scan data are now being analyzed to determine whether or not any rate data can be obtained.

The capsule was sectioned into three parts: one containing the pellet, one containing the sodium, and the section of tube above the sodium. Each of these parts was counted with a 1 in. x 1 in. x 0.2 in. lithium-drifted, germanium solid-state crystal. The sodium tube and tube above the sodium were placed as close as possible to the crystal while the pellet was positioned 21 in. from the crystal. In addition, to obtain absolute count rates, the sodium section and the tube above the sodium were counted in an annular NaI crystal which was 12 in. long, 2-1/2 in. i.d. and 8 in. o.d.

All three of the solid-state counts showed peaks of ^{131}I, ^{137}Cs, ^{95}Zr, ^{95}Nb, ^{103}Ru, and ^{140}Ba-^{140}La. When the pellet was dropped into the 12 in. capsule, very small amounts of Pu-U carbide must have rubbed off on the walls. Thus, all of these fission products were found at all positions, even 8 in. above the sodium level. Therefore, the count of the section above the sodium allowed corrections to be made for the rub-off effect.

A check on the total number of fissions in the pellet was possible by multiplying the ^{137}Cs or ^{131}I peak counts found in the pseudo 4 π NaI count by the peak ratios of pellet to sodium found by the solid-state crystal. This number was then corrected for geometry and decay. The results showed the data to be internally consistent since the estimated fissions calculated from flux and the fissions from the count rate calculation agreed to within 5%.

By combining the integrated results from the 4 π NaI count with the sharp peak definition of the solid-state crystal count, the concentrations of fission products which transferred to the sodium could be determined. The results are as follows:

	Ratio of Atoms in Pellet to Atoms in Na	Atoms in Na at End of Run	Conc. in Na at End of Run (ppm)
^{131}I	3360	8.7×10^{8}	2.6×10^{-8}
^{137}Cs	3810	5.9×10^{11}	1.8×10^{-5}
^{140}Ba	875000	5.1×10^{7}	1.7×10^{-9}

The scans indicated that the following fission products did not transfer into the sodium: ^{95}Nb, ^{95}Zr, and ^{103}Ru.

The low level of mass transfer indicates that the controlling mechanism may be the solid-state diffusion of the fission product out of the carbide pellet. To check this assumption, a penetration thickness was calculated which accounted for the ^{137}Cs atoms lost by the pellet. The concentration profile down to within 1% of the pellet-edge concentration was integrated to obtain the penetration thickness. This distance is directly associated with the diffusivity. The results are as follows:

Penetration thickness = 5.17×10^{-5} cm

^{137}Cs diffusion coefficient = 3.3×10^{-17} cm^2/sec.

The diffusion coefficient compares favorably with the diffusion coefficient found in uranium oxide pellets. The following coefficients at 750°C have been determined.[1]

^{131}I : $D = 3.5 \times 10^{-16}$ cm^2/sec
^{133}Xe: $D = 5 \times 10^{-17}$ cm^2/sec

The general agreement between the calculated diffusivity and those for UO_2 pellets indicates that the assumption of solid-state diffusion control is probably correct.

III. TRANSPORT AND DISTRIBUTION OF FISSION PRODUCTS IN SODIUM: LOOP EXPERIMENTS (J. C. Clifford)

A. General

Long-lived fission products are added to a small, forced-convection sodium loop by immersing irradiated plutonium-base fuel in sodium. Migration of activity from the fuel to removable specimens and traps is detected by *in situ* gamma-ray spectrometry and by radiochemical analyses of the adsorbers and traps after test.

B. Current Results

A full-flow sodium oxide cold trap was operated in the fission-product distribution loop for approximately 2900 hr between the temperatures of 110° and 200°C. At the end of this period, the cold trap was removed and dissected and several portions were analyzed for total ^{90}Sr, ^{137}Cs, ^{155}Eu, ^{144}Ce, ^{60}Co, Pu, and ^{125}Sb content. These analyses have not been completed. At the same time two activity collectors, consisting primarily of stainless steel mesh, were removed from the system for radiochemical analyses. One surface had been maintained at 500°C during the full-flow sodium oxide trap experiment and the other at approximately 310°C. Gross measurement of beta and gamma activities indicated that significant segregation had occurred, with the low temperature surfaces exhibiting 10 times the gamma activity and 3 times the beta activity found on the higher temperature surfaces. Samples of sodium were withdrawn from the loop at the end of the test and preliminary radiochemical analyses showed the following levels.

Species	Specific Activity in Na (d/m/g Na)	Equivalent Concentration in Na (ppm)
^{137}Cs	2×10^6	0.01
^{90}Sr	1×10^4	3×10^{-5}
Pu	--	≤ 0.1

Activity of ^{155}Eu in the samples was approximately half that of ^{90}Sr; ^{144}Ce, ^{125}Sb, and ^{106}Ru either were not detected or were present in trivial amounts.

Gamma spectra were obtained of the fission product source (irradiated Pu-Co-Ce alloy) for this experiment before and after test: they showed that only 60% of the ^{137}Cs available in the fuel was extracted to the sodium phase at 500°C.

A diffusion cold trap has been inserted in the forced-convection loop and is being used to scavenge residual fission products from the system.

IV. TRANSPORT AND DISTRIBUTION OF FISSION PRODUCTS IN SODIUM: CAPSULE EXPERIMENTS (J. M. Williams)

A. General

Capsule experiments have been designed to determine the distribution of gamma-active isotopes in the sodium/stainless steel/helium/adsorber system as a function of time and temperature. The use of gamma-ray scanning techniques will enable the study of transport rates, adsorption and desorption phenomena, and the equilibrium distribution between phases. The isotope ^{137}Cs is the first radioisotope to be studied in these experiments because it is a major fission product released from irradiated nuclear fuels and its 27.7 yr half-life is relatively long. Other candidates for study, using these experimental techniques, are ^{131}I and ^{140}Ba-^{140}La.

B. Current Results

A capsule furnace has been built and operated to heat a nominal 8-in.-long, 1-in.-diameter stainless steel capsule containing sodium and 1 mC of ^{137}Cs. The necessary gamma-ray scanning hardware and electronics for determining ^{137}Cs distributions have been assembled. The arrangement of the experimental scanning apparatus (Fig. 1) is such that the detector and shield pig remain stationary while the capsule and furnace can be moved in any direction in one mil increments.

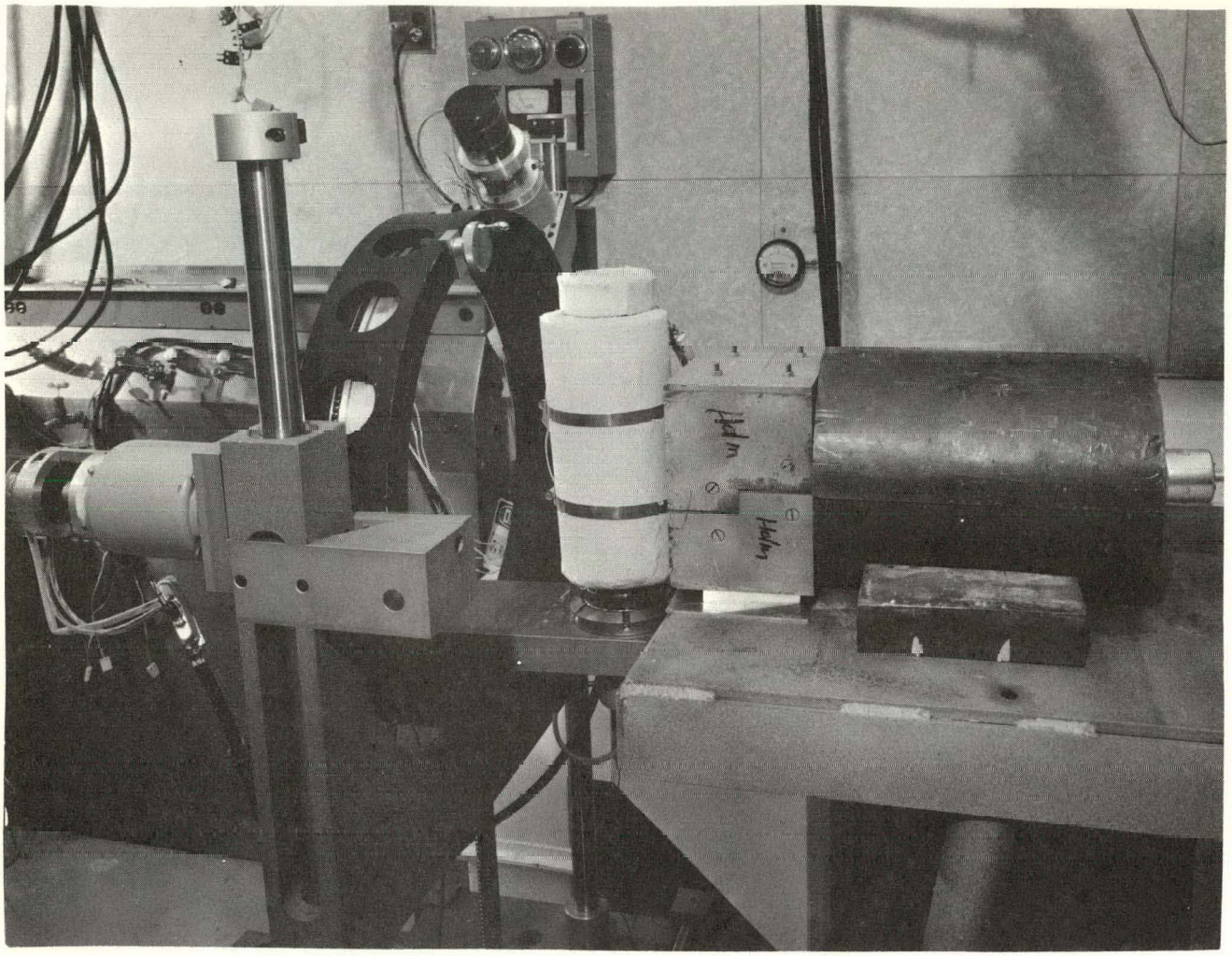

Fig. 1 Gamma Scanning Arrangement Showing Capsule Furnace, Stationary Detector System, and Mechanical Positioning Device.

Initial studies with this experimental apparatus are being devoted to optimizing methods for quantitative determination of spatially distributed sources.

References

1. Japan-U. S. Research Newsletter, "Oxide and Carbide Fuels," No. 4, December 1965. Compiled by The Atomic Energy Bureau, Kasaumigaseki, Tokyo, Japan, pp A9-150.

PROJECT 802

MEASUREMENT OF IMPURITIES AND DEVELOPMENT OF QUALITY CONTROL TECHNIQUES FOR HIGH TEMPERATURE SODIUM COOLANT SYSTEMS

Person in Charge: D. B. Hall
Principal Investigators: R. H. Perkins
V. J. Rutkauskas

I. INTRODUCTION

The design criteria and performance requirements for the LMFBR and the experimental test facilities in support of that program require investigation in the area of sodium-coolant chemistry so that the problems associated with the identification and control of the significant chemical reactions occurring in the sodium coolant can be more fully understood. The objectives of this investigation are:

1. Determination of the solubility of oxygen in sodium as a function of temperature using the vacuum-distillation analytical technique.
2. Development of dynamic in-line sodium-sampling techniques for the vacuum-distillation analytical method. The intent of this phase of the program is to develop a prototype sampling system capable of extracting representative sodium samples from engineering systems for the analysis of all dissolved impurities, including fission-product elements. With minor modification this sampling system will have the capability of being used in a radioactive sodium environment.
3. Development and evaluation of prototype in-line analytical instrumentation for the continuous monitoring of oxygen and/or gaseous and metallic impurities of interest in sodium systems.
4. Evaluation of the (γ,n) activation technique for the determination of oxygen and carbon in sodium and other activation analytical techniques for impurities in sodium.
5. Evaluation of the lowest oxygen levels which can be practically maintained for the cold-trap and hot-trap mode of quality control.
6. Development and evaluation of techniques utilizing soluble "getters", i.e., Mg, Ca, and Ba as quality control mechanisms for maintaining system oxygen concentrations, and the development of analytical methods required to evaluate and monitor this particular mode of quality control. This technique has the potential for effectively controlling not only O, but C, H, N, and possibly metallic fission-product elements and other metallic impurities.

II. IMPURITY ANALYSIS AND SAMPLING STUDIES (V. J. Rutkauskas)

A. General

Dynamic in-line sodium sampling techniques for the vacuum-distillation analytical method are presently being evaluated. The objective of this phase of the program is to develop a prototype sampling system for engineering systems and reactor application and the development of in-line analytical techniques and alternate analytical techniques to complement the vacuum-distillation technique.

Although the vacuum-distillation method has many advantages over the more widely accepted techniques for impurity analyses in sodium, there are a number of problem areas which must be investigated to assess the over-all capabilities of the method. Of prime importance are the nature of the residues following a distillation and the effects of distillation temperatures on the nature of the residues. The distillation residues may contain compounds composed of various combinations of sodium, oxygen, carbon, and fission-product elements, and measurement of alkalinity or sodium content may be mis-

leading as measures of oxygen assumed to be totally present as Na_2O.

The (γ,n) activation technique for the determination of carbon and oxygen in sodium has the capability for measuring oxygen specifically rather than relating the oxygen content to total alkalinity or sodium content. This method is theoretically capable of determining the concentrations of these elements directly with a sensitivity of < 1 ppm. It should also provide a very useful tool for evaluating the distillation method for oxygen analysis and shed some light on the nature of the residues. Additional methods for the determination of other impurities of interest will require a continuing development effort.

The solubility of oxygen in sodium using the vacuum-distillation analytical technique has been evaluated over the temperature range of 125° to 300°C. This investigation was conducted in a dynamic system (Analytical Loop No. 1) using a cold trap as the mechanism for oxygen control. The results of this investigation were published in the first quarterly report of last year.

B. Current Results

The Analytical Loop No. 1 experimental facility has been relocated in the sodium experimental area of the building. A number of modifications are being made to the integral vacuum-distillation sampling system and the dynamic facility is being modified to accept the full-flow vacuum-distillation sampling system.

A technique has been developed for trapping evolved gases released during the vacuum-distillation of sodium. The procedure involves a cryogenic trap on the vacuum system of the distillation apparatus and subsequent elution of the gas sample to a gas chromatograph. Ninety-five per cent recovery of known impurities added to the vacuum system have been obtained using this trapping technique. Information on the quantity and composition of any gases released during a distillation analysis is necessary in order to evaluate the effects, if any, of the time and temperature of distillation on the nature of the residues and to determine if this technique is applicable for the determination of carbon in sodium. Preliminary results have indicated that portions of the vacuum/inert-gas system associated with the integral vacuum-distillation sampler have been acting as sources of gaseous impurities. As a result, the entire vacuum/inert-gas manifolding system associated with the distillation samplers has undergone extensive re-design for which the bulk of the purchased equipment has been received and most of the manifold modules have been fabricated.

Approximately 75% of the mechanical design for the Analytical Loop No. 2 experimental facility has been completed and the construction drawings for the main driver loop and bulk sodium tank containing the jet-pump mixing chamber have been submitted for fabrication. This facility will be used for the development of soluble gettering techniques and the development and evaluation of prototype in-line analytical instrumentation for the continuous monitoring of oxygen and/or other gaseous and metallic impurities of interest in sodium systems.

Approximately 60% of the mechanical design has been completed for the experimental facility which will be used in the carbon-analysis and residue-identification programs. The program to evaluate analytical methods for the determination of carbon in sodium in the range of 1 to 10 ppm has been broadened to include residue identification.

A continuing effort is being maintained to develop atomic-absorption spectrophotometric analytical procedures for the determination of trace-level metallic impurities (other than sodium) remaining in the residue and the condensate following a distillation. In addition, procedures to determine trace metallic impurities in bulk sodium samples by the same method are also being investigated.

A new detector system is being designed and procured for use in evaluating photon activation as a technique for determining carbon and oxygen in sodium. Read-search capability and multiparameter operation are being added to the analyzer system. The read-search makes it possible to read back data from the magnetic tape into the analyzer. This permits the addition of data to a previous spectrum and lets the experimenter make sure that the data are actually going on tape. Multiparameter operation will make it possible to measure the total energy absorbed in the detectors, assisting in the reduction of interferences. Low background lead has been received for a shield around the NaI detectors.

PROJECT 803

KINETICS OF SODIUM COLD TRAPS

Person in Charge: D. B. Hall
Principal Investigators: R. H. Perkins
C. C. McPheeters

I. INTRODUCTION

Control of oxygen concentration in sodium can be accomplished by precipitation of sodium oxide at low temperatures in a cold trap. It is the purpose of this project to determine the parameters necessary for successful design of cold traps for systems of any size or required oxygen removal rate. The data will be obtained from experimental cold traps of various sizes and degree of packing. The variables of flow rate, system oxygen concentration, temperature, oxygen content of the cold trap and cold trap temperature will be considered. The data will be used to establish a theoretical model to analytically describe the mechanisms of cold trap operation. The end result of the project will be a cold trap design manual.

II. COLD TRAP TEST LOOP
(C. C. McPheeters)

A. General

The cold trap test loop (Fig. 1) is an isothermal, forced convection sodium system which consists of a ballast tank, a cold trap section and associated piping, expansion tank and NaK coolant circuit. Sodium will be pumped from the ballast tank through an analytical section where a United Nuclear Corporation oxygen meter, a vacuum distillation sampler, and a plugging meter will be used to analyze the sodium for oxygen. The sodium will then pass through the cold trap section which will accommodate replaceable cold traps of various design. From the cold trap section, the sodium will flow through an expansion tank to a second United Nuclear Corporation oxygen meter and back to the ballast tank.

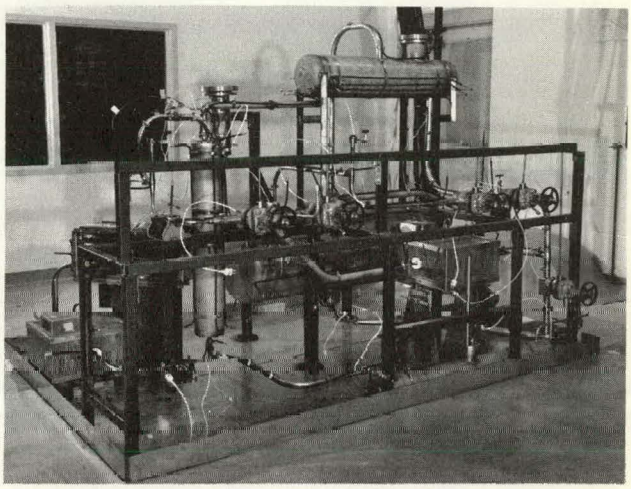

Fig. 1. Cold Trap Test Loop.

Performance tests will be run on simple cold trap designs of various sizes and degrees of packing. The performance tests will consist of a rapid removal of oxygen from the test loop by the cold trap. Oxygen concentration will be measured as a function of time.

B. Current Results

Construction of the test loop has been completed, and all heaters and thermocouples have been installed. Insulation of the loop should be completed in one week. Electrical wiring of the heater circuits and thermocouples should require an additional two weeks for completion. Heater power supplies, temperature recorders and other necessary instrumentation have been completed (Fig. 2). The test loop will be filled with sodium in about five weeks.

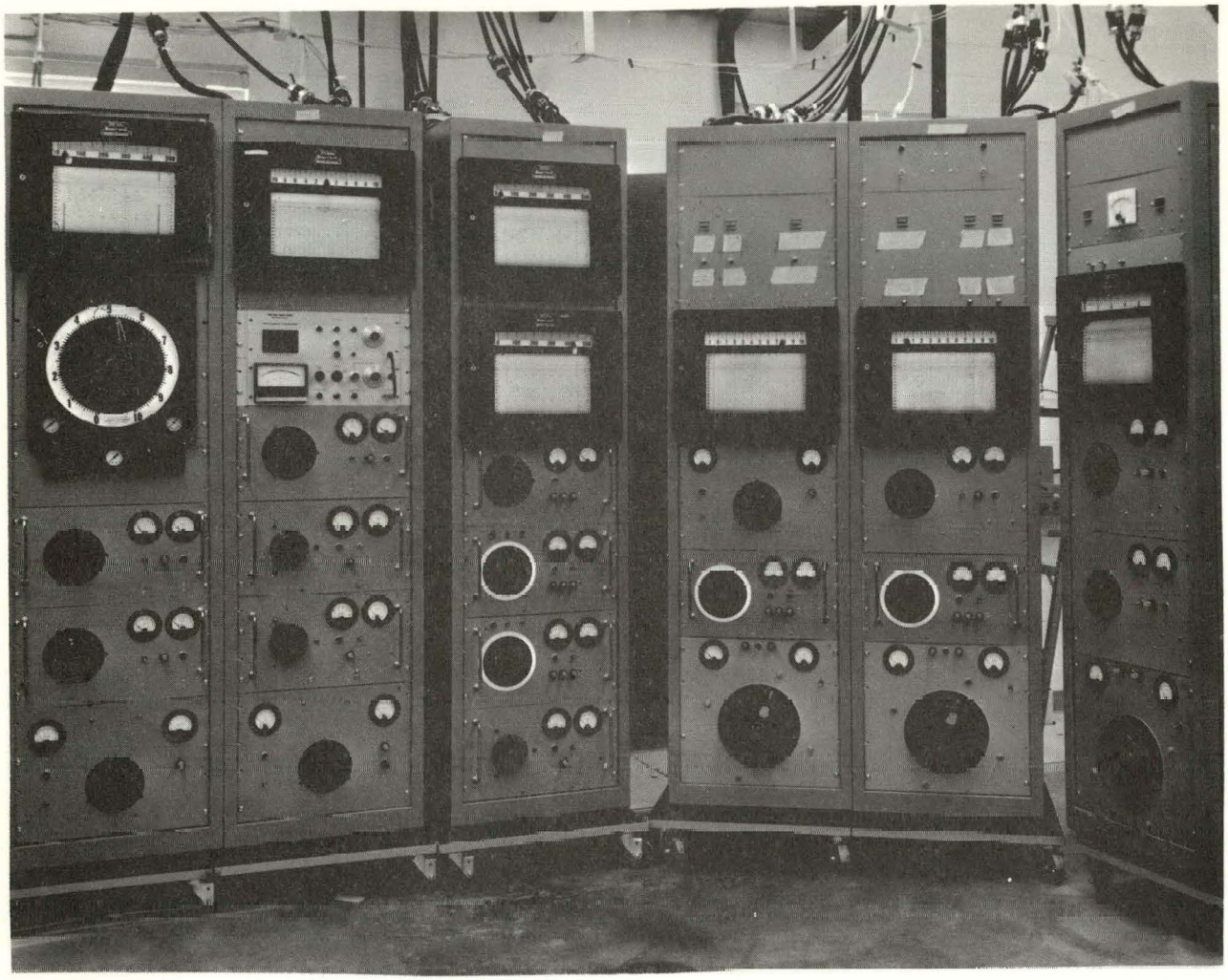

Fig. 2. Cold Trap Test Loop Instrumentation Racks.

The expected performance characteristics of the simple cold trap design to be used in the first tests will be predicted based on past experience both at LASL and other locations. Although the design is quite simple, the mathematical analysis of the expected mechanisms of sodium monoxide precipitation is complex. For this reason a computer code will be used to divide the cold trap into regions which will be treated as individual cold traps at different temperatures and in series. Such an analysis will yield not only the expected rate of cleanup of the system as a function of time, but also the expected location and form of the oxide in the cold trap.

Tests on the first cold trap design should be started during the next reporting period.

PROJECT 807

CERAMIC PLUTONIUM FUEL MATERIALS

Person in Charge: R. D. Baker

Principal Investigator: J. A. Leary

I. INTRODUCTION

The principal goals of this project are to prepare pure, well characterized plutonium fuel materials, and to determine their high temperature properties. Properties of interest are (1) thermal expansion, (2) thermal conductivity, (3) thermal stability, (4) phase relationships by differential thermal analysis, (5) structure and phase relationships by x-ray diffraction, high temperature x-ray diffraction, neutron diffraction and high-temperature neutron diffraction, (6) density, (7) hardness and its temperature dependence (8) compatibility including electron microprobe analysis, (9) compressive creep (deformation).

In addition to phase equilibria and general properties, specific thermodynamic properties such as free energy of formation by vaporization equilibria in the 1000-2000°C temperature range with mass spectrometer identification of vapor species, free energy of formation by electromotive force measurement in the 450-1200°C temperature range, and heat capacity and heat of transition at temperatures up to 2900°C are being determined.

II. SYNTHESIS AND FABRICATION

(M. W. Shupe, R. L. Nance, R. W. Walker, T. K. Seaman)

1. Carbides

Approximately 1 cm. dia rods of the monocarbides $(U_{0.90}Pu_{0.10})C$, $(U_{0.80}Pu_{0.20})C$, $(U_{0.70}Pu_{0.30})C$, and $(U_{0.15}Pu_{0.85})C$ were prepared by arc casting and solution treating. In addition, rods of $(U, Pu)_2C_3$ plus excess carbon were prepared having U/Pu atomic ratios of 95/5, 90/10, 80/20, 50/50, 10/90. Dicarbides having the U/Pu atomic ratios of 90/10, 85/15, 80/20, 60/40, 50/50, 25/75, and 10/90, plus a slight excess of carbon also were prepared. All of these specimens were used for differential thermal analysis.

The reduction of $(U_{0.80}Pu_{0.20})C_{1.2}$ powder to stoichiometric monocarbide by H_2 was discussed in a previous report. It is advantageous if this reaction essentially stops at a C/M ratio of 1.00, otherwise the reaction will be difficult to control on a routine basis. In order to evaluate this, a second "reduction" cycle was completed starting with stoichiometric monocarbide. Within the limits of analytical error, there was no reduction in the C/M ratio in this experiment. Additional preparations will be done on the 50 g. scale.

2. Nitrides

UN or PuN powders have been cold compacted to 1 cm. dia pellets and sintered to high densities (> 90 percent of theoretical) by conventional methods. When the UN and PuN powders are blended, pressed and sintered, single phase, solid solution pellets result as discussed in previous reports. However, the maximum densities obtained with sintered solid solution pellets of the composition $U_{0.80}Pu_{0.20}N$ has been 88 percent of theoretical. Regrinding the solid solution nitride pellets to -325 mesh powder, followed by compaction and sintering for 3.5 hr at 1750°C in Ar did not significantly increase pellet density.

The effect of oxygen on the lattice dimension of (U, Pu)N solid solutions is being determined. Powders of $(U_{0.80}Pu_{0.20})N$ plus 2 percent by wt. $(U_{0.80}Pu_{0.20})O_2$ were pressed and sintered for 4 hr in Ar. The lattice dimension of the mononitride was increased from 4.892A

to 4.908A by this treatment. Additional experiments with varying U/Pu ratios indicate that large positive deviations from Vegard's law are obtained for (U, Pu)N solid solutions that have incorporated significant amounts of oxygen in the lattice.

III. PROPERTIES

1. Differential Thermal Analysis

(J. G. Reavis)

Additional measurements have been made of transition temperatures by differential thermal analysis of U-Pu-C samples. Supporting evidence has come from metallographic and x-ray analysis of these samples. A study of reproducibility has been made to insure the accuracy of the observations.

Reproducibility of Measurements: Transitions of five of the standard reference materials observed during the early stages of this work (LA-3601-MS) have been remeasured. The observed transition temperatures were corrected for light absorption of the components of the optical system as determined about one year ago. Table I shows a comparison of these corrected values with literature values and with values determined during early stages of this work.

Table I

DTA Apparatus Calibration Check

Transition	Temperature, °C Early	Recent	Literature
Pt +C, m.p.	1735	1739	1734
Pt, m.p.	1760	1777	1770
Rh, m.p.	1970	1960	1966
$MoC_{0.2}$ eutectic	2200	2210	2205
Ir, m.p.	2440	2445	2440

It can be seen from these values that after prolonged use of the DTA system transition temperatures still fall within a ± 10° uncertainty range.

As a further reproducibility check of the entire procedure of measurement of transition temperatures of carbides (including sample preparation), new MC_{2+x} samples with the same nominal U/Pu ratios as previously-observed samples were observed. In some samples the amount of excess C in the sample was also varied to determine if this produced a measurable effect. Results of this series of observations are shown in Table II.

Table II

Transition Temperatures of (U, Pu)C_2 Samples Checking Reproducibility and the Effect of Excess C

Nominal Composition	Transition Temp., °C 1st	2nd
Recent observations		
$Pu_{0.1}U_{0.9}C_3$	1695	2445
$Pu_{0.1}U_{0.9}C_2$	1695	2440
$Pu_{0.25}U_{0.75}C_3$	1720	2400
$Pu_{0.5}U_{0.5}C_3$	1745	2335
$Pu_{0.5}U_{0.5}C_4$	1745	2345
Earlier observations		
$Pu_{0.1}U_{0.9}C_3$	1705	2445
$Pu_{0.25}U_{0.75}C_3$	1725	2410
$Pu_{0.5}U_{0.5}C_4$	1745	2340

These values indicate the reproducibility range is about ±10°C. It is also seen that the transition temperatures are not appreciably changed by further addition of C to stoichiometric MC_2.

Additional Observations on MC_{2+x} Compositions: In addition to the MC_{2+x} samples discussed in the preceding paragraph, other samples having different U/Pu ratios have been observed and are listed in Table III.

Table III

Transitions Observed by DTA for (U, Pu)C_{2+x}

Nominal Composition	Transition Temp., °C 1st	2nd
$Pu_{0.05}U_{0.95}C_3$	1745	2465
$Pu_{0.15}U_{0.85}C_3$	1665, 1705	2420
$Pu_{0.4}U_{0.6}C_3$	1745	2350

Except for the composition range 0-20 mole percent PuC_2, the DTA results obtained to date define the MC_2/M_2C_3 + C transition and MC_2 melting boundaries.

2. X-ray Powder Diffraction

(C. W. Bjorklund, R. M. Douglass, R. L. Nance)

Work is continuing on x-ray powder diffraction studies of uranium-plutonium fuel materials. A good pattern was obtained for an annealed solid solution containing approximately 90% PuC_2-10% UC_2. The pattern was similar to those obtained previously for samples of nominally 100% PuC_2 composition with better resolution in the high angle region. It was possible to corroborate

the presence of phases previously identified as dicarbide, sesquicarbide, monocarbide, oxide, graphite, and one or more as yet unidentified phases. Samples of Pu_2S_3, before and after annealing in H_2 at 950°C, have been identified as orthorhombic α-Pu_2S_3. An attempt is being made to determine whether the pattern corresponds to that of the αPu_2S_3 cell reported by Marcon and Pascard[1] for which only limited data is available, or the smaller cell reported[2] for αGd_2S_3, with which α-Pu_2S_3 is believed to be isomorphous.

Additional data have been obtained in the study of self-irradiation damage in plutonium ceramics. The lattices of plutonium oxides, carbides and nitrides of "normal" isotopic composition continue to expand at a nearly steady rate after periods of 500 to 1300 days. The lattice dimensions of samples of PuC containing Pu enriched with 4 atom % Pu-238 increased rapidly at first but are now beginning to decrease steadily with time. This effect has been observed for both a single phase PuC sample and PuC in equilibrium with Pu_2C_3. The lattice of the Pu_2C_3 phase is still expanding slowly. The quality of the powder patterns is also deteriorating, but it is too early to attempt to determine the cause. Radiation damage to samples of PuO_2 (in which the Pu contains 3.75 atom % Pu-238) stored at temperatures between -200° and 400°C has leveled off sufficiently to apply a least squares curve-fitting technique to the data. The following equations were obtained, where Δa is the increase in the value of the lattice dimension from the original value, a_o, at time o, and t is the time in days:

PuO_2 at -200°C $\frac{\Delta a}{a_o} = 3.15 \times 10^{-3} (1-e^{-0.0128t})$

PuO_2 at 25°C $\frac{\Delta a}{a_o} = 3.05 \times 10^{-3} (1-e^{-0.0131t})$

PuO_2 at 100°C $\frac{\Delta a}{a_o} = 2.84 \times 10^{-3} (1-e^{-0.0129t})$

PuO_2 at 200°C $\frac{\Delta a}{a_o} = 2.35 \times 10^{-3} (1-e^{-0.0154t})$

PuO_2 at 400°C $\frac{\Delta a}{a_o} = 1.77 \times 10^{-3} (1-e^{-0.0172t})$

The samples were stored in glass or quartz capillaries and brought to room temperature for each x-ray exposure.

3. High Temperature X-ray Diffraction
(J. L. Green)

Fabrication of the major components of the furnace for the Picker diffractometer is essentially complete. Photographs of the partially assembled furnace are shown in figures 1 and 2. (The Be window is not shown.) The

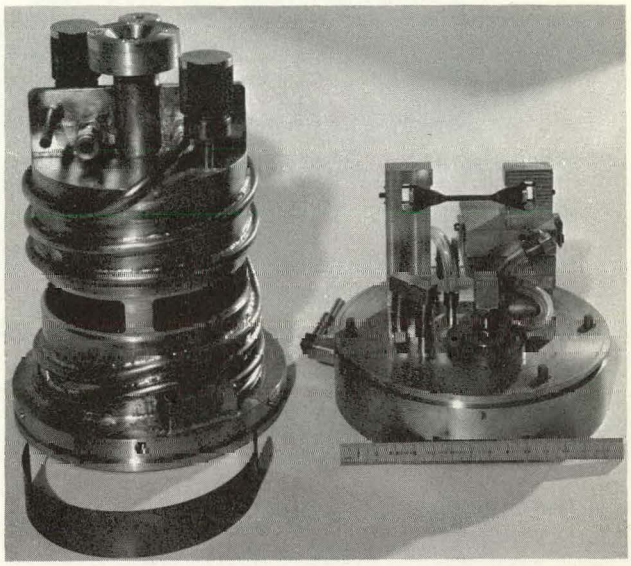

Fig. 1. Components of High Temperature Furnace for X-ray Diffractometer.

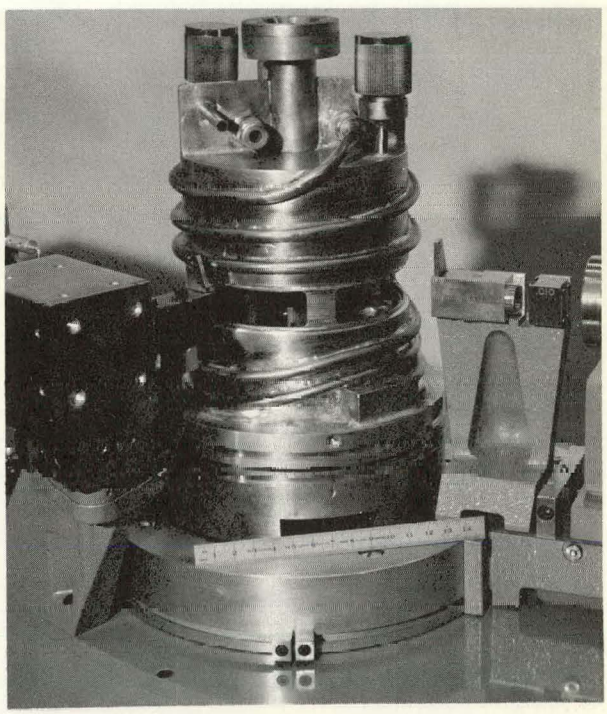

Fig. 2. High Temperature Furnace Shown in Position on X-ray Diffractometer (before installation of Be window).

sample is supported on a resistance heated graphite strip to produce a hot zone 0.1 in. high by 1 in. long. The strip in turn is supported and aligned by two water cooled posts which are pinned to a massive brass base having a dovetail slot to receive the sample track of the diffractometer. One of the mounting posts is stationary while the other is given lateral freedom. This system allows for the relatively large dimensional changes in the heater strip due to thermal expansion and at the same time precisely maintains the proper orientation of the sample surface with respect to the diffractometer. The enclosure of the sample area is made complete by a water cooled brass can. The x-ray beam enters and leaves the furnace through a 0.020 in. thick Be window sealed to the can. View ports are located on the top and rear of the can to allow pyrometric temperature measurements and visual observation of the sample area. Electrical power to the furnace is supplied by a regulated 4 KVA power supply.

4. Neutron Diffraction
(J. L. Green)

Final calculations from the low temperature neutron diffraction study on PuC have been completed. The scattering amplitude for Pu^{240} was found to be 0.36 ± 0.05. This value will be refined at a later date by investigating the scattering characteristics of PuO_2.

Based on the antiferromagnetic ordered structure of PuC described previously and quantitative intensity data, it was possible to compute a quantity approximating the magnetic moment of the plutonium ions involved in the ordered structure.

$$gJf = 0.67 \pm 0.05 \text{ Bohr magnetons}$$

where gJ is the magnetic moment and f is the magnetic form factor. Sufficient data are not available to evaluate f; however, the data from this study showed no systematic decrease in gJf with increasing angle within the limits of experimental error. This would tend to indicate that f is a slowly varying function of angle in the angular region involved in this study. Therefore, gJf would not be expected to be substantially smaller than gJ, the magnetic moment. This being the case, the measured moment appears to be most consistent with a cation lattice made up of Pu^{+3} ions.

5. Thermocynamic Properties from EMF Cells
(G. M. Campbell and L. J. Mullins)

Six additional cells of the type Pu_2C_3 + C/Pu^{+3}, LiCl-KCl/$PuRu_2$ + Ru have been assembled and monitored. Although three of these cells were very stable the EMF did vary from cell to cell by as much as 25 mv. This corresponds to a variation in the free energy of formation of Pu_2C_3 of 3.4 kcal/mole. During this period the same Pu-Ru alloy reference electrode gave very precise results on three cells where its EMF was measured against that of liquid Pu. There was no evidence of variation from cell to cell. Reasons for the variation in the EMF of the carbide cells are being investigated.

A double chamber EMF cell has been used to measure the potential of the cell

Pu, $PuCl_3$ (s)/$BaCl_2$ (s)/AgCl-NaCl, Ag (s)

The double chamber cell eliminates the possibility of mass transfer via the gas phase between the electrodes. Measurements with the double chamber cell agree with those obtained in a single chamber cell (LA-3607-MS) to within ~5 mv. EMF values obtained at 550°C with both cells are compared in Table IV.

Table IV

Comparison of Cell Potentials

Exp't	Cell Type	E, volts
S-7	Single chamber	1.709
S-9	Single chamber	1.689
S-11	Double chamber	1.705
S-12	Double chamber	1.704

When these values are combined with literature data for the cell

Ag (s)/AgCl, NaCl (s)/Cl_2 (g)

a standard free energy of formation of 182.7 (± .4) kcal/mole is obtained for $PuCl_3$ at 550°C.

Work is now in progress on the solid electrolyte cell

Mg, MgF_2 (s)/CaF_2 (s)/Pu, PuF_3 (s)

This cell will be monitored over the temperature range 430-630°C. This cell should yield thermodynamic data

for PuF_3 and will serve as a guide for the operation of high temperature cells (600-1000°C) for ceramic plutonium compounds.

6. Thermodynamic Properties from Vaporization Studies (R. A. Kent)

The defective quadrupole section of the high temperature mass spectrometer was realigned by the manufacturer (Electronic Associates, Inc.) and returned to LASL. Calibration experiments were initiated and it was observed that the ionization section of the mass spectrometer was of a poor design, the tungsten wire filament frequently shorting out. Consequently a new ion source was designed, tested and installed.

In order to test the apparatus for vapor pressure measurements of high molecular weight species by means of the Knudsen technique, three experiments were conducted in which the ion current (I) of the gold peak ($^{197}Au^+$) was measured as function of temperature T in °K. In each of the three experiments the sample consisted of melted gold wire of 99.98% purity contained in a graphite Knudsen cell in a Ta shell. Temperatures were measured by sighting into a black body hole in the side of the Knudsen cell with a micro-optical pyrometer. The data for the three experiments are presented in Table V.

The electron multiplier detector is so designed that its gain may be measured and the values of I^+T for experiments A, B and C were normalized to take into account changes in multiplier gain. The data for experiments A and B were taken at an ionizing voltage of 70 e.v. The data for experiment C were taken at 25 e.v. and were normalized to those taken at 70 e.v.

A plot of the data in the form log I^+T vs 1/T leads to the least-squares equation

$$\log (I^+T) = -(18158 \pm 415)/T + (7.056 \pm 0.199) \quad (1)$$

The slope of the line obtained from equation (1) is essentially the same as that obtained for Au(liq) by Ward[3] in his Knudsen-target collection experiments. The machine constant K was calculated from the equation

$$P = K(I^+T) \quad (2)$$

by combining equation (1) with the corrected least-squares equation of Ward to yield $K = 6.37 \times 10^{-2}$ atm/amp. deg. K.

Equation (1) then becomes

$$\log P_{atm} = -(18158 \pm 415)/T + (5.860 \pm 0.199) \quad (3)$$

Values of log P_{atm} obtained from equation (3) were combined with free-energy functions for Au (ℓ) and Au(g) tabulated by Stull and Sinke[4] to obtain the third law values of ΔH°_{298} presented in Table V. The scatter in the values for experiment A is due in part to the fact that the power supply used to heat the Knudsen cell was not regulating. This unit was repaired before experiments B and C were run. The remainder of scatter is due primarily to the instability of the mass spectrometer electronics.

The second law enthalpy corrected to 298°K is $\Delta H^\circ_{298} = 88.37 \pm 1.90$ kcal mole^{-1} which agrees well with the third law value of $\Delta H^\circ_{298} = 88.48 \pm 0.54$ kcal mole^{-1}. These values are compared with the third law values obtained by other workers in Table VI.

Table VI

Comparison of Third Law Heats of Vaporization of Au

Reference	ΔH°_{298} kcal mole^{-1}
Ward[3]	88.5 ± 0.2
Hildebrand and Hall[5]	88.3 ± 0.3
Edwards in ref (6)	87.0
Rauh in ref (6)	87.2 ± 0.8
Nesmeyanov in ref (6)	87.6
This work	88.48 ± 0.54

In addition, the second law value of $\Delta S^\circ_{298} = 31.7 \pm 0.9$ e.u. compares well with that obtained from Wards data 32.0 e.u., and the values listed by Stull and Sinke[4] and Hultgren[6], 31.80 e.u. and 31.81 e.u., respectively.

From the above data, the value of ΔH°_{298} for gold is recommended to be 87.8 ± 1.0 kcal mole^{-1}.

These and other preliminary experiments have indicated that the modified Residual Gas Analyzer spectrometer will be adequate for use in the uranium and plutonium mass regions. Although sensitivity and stability are acceptable, resolution will not be as good as expected.

Table V

Vapor Pressure Data for Gold (liq.)

Point	Temp., ^{o}K	$10^{4}/T^{o}K$	$-\log I^{+} T$	$-\log P$	P_{atm}	$-\Delta\left(\frac{F_T^o - H_{298}^o}{T}\right)$ e.u.	ΔH_{298}^o kcal. mole^{-1}
A1	1612	6.203	4.291	5.487	3.26×10^{-6}	30.17	89.11
A2	1629	6.139	4.109	5.305	4.96×10^{-6}	30.13	88.63
A3	1642	6.090	4.039	5.235	5.69×10^{-6}	30.12	88.80
A4	1664	6.010	3.943	5.139	7.26×10^{-6}	30.07	89.17
A5	1671	5.984	3.777	4.973	1.06×10^{-5}	30.06	88.26
A6	1691	5.914	3.668	4.864	1.37×10^{-5}	30.02	88.41
A7	1627	6.146	4.218	5.414	3.85×10^{-6}	30.14	89.34
A8	1587	6.301	4.468	5.664	2.17×10^{-6}	30.22	89.09
A9	1562	6.402	4.583	5.779	1.66×10^{-6}	30.27	88.58
B1	1665	6.006	3.830	5.026	9.42×10^{-6}	30.06	88.34
B2	1657	6.035	3.854	5.050	8.91×10^{-6}	30.08	88.14
B3	1647	6.072	3.907	5.103	7.89×10^{-6}	30.10	88.03
B4	1648	6.068	3.987	5.183	6.56×10^{-6}	30.10	88.70
B5	1629	6.139	4.107	5.303	4.98×10^{-6}	30.13	88.62
B6	1606	6.227	4.287	5.483	3.29×10^{-6}	30.17	88.75
B7	1581	6.325	4.479	5.675	2.11×10^{-6}	30.23	88.85
C1	1766	5.663	3.224	4.420	3.80×10^{-5}	29.87	88.46
C2	1784	5.605	3.173	4.369	4.28×10^{-5}	29.84	88.90
C3	1756	5.695	3.226	4.422	3.78×10^{-5}	29.89	88.03
C4	1723	5.804	3.417	4.613	2.44×10^{-5}	29.95	87.98
C5	1743	5.737	3.396	4.592	2.56×10^{-5}	29.92	88.77
C6	1756	5.695	3.268	4.464	3.43×10^{-5}	29.89	88.36
C7	1788	5.593	3.094	4.290	5.13×10^{-5}	29.83	88.43
C8	1763	5.661	3.218	4.414	3.85×10^{-5}	29.88	88.29
C9	1741	5.744	3.323	4.519	3.03×10^{-5}	29.92	88.09
C10	1723	5.804	3.417	4.613	2.44×10^{-5}	29.95	87.98
C11	1694	5.903	3.634	4.830	1.48×10^{-5}	30.01	88.27
C12	1677	5.963	3.735	4.931	1.17×10^{-5}	30.03	88.19
C13	1645	6.079	3.943	5.139	7.26×10^{-6}	30.10	88.20
C14	1644	6.083	3.959	5.155	7.00×10^{-6}	30.11	88.28
C15	1627	6.146	4.099	5.295	5.07×10^{-6}	30.14	88.46
C16	1599	6.254	4.260	5.456	3.50×10^{-6}	30.19	88.20
C17	1568	6.378	4.478	5.674	2.12×10^{-6}	30.26	88.15
C18	1544	6.477	4.623	5.819	1.52×10^{-6}	30.30	87.90
C19	1530	6.536	4.839	6.035	9.37×10^{-7}	30.34	88.68
C20	1512	6.614	4.921	6.117	7.64×10^{-7}	30.37	88.24
C21	1484	6.739	5.195	6.391	4.06×10^{-7}	30.44	88.58
C22	1464	6.831	5.320	6.516	3.05×10^{-7}	30.48	88.28
C23	1445	6.920	5.548	6.744	1.80×10^{-7}	30.52	88.69
C24	1440	6.944	5.554	6.750	1.78×10^{-7}	30.54	88.46
C25	1414	7.072	5.818	7.014	9.68×10^{-8}	30.60	88.66
C26	1386	7.215	6.084	7.280	5.25×10^{-8}	30.66	88.66
C27	1377	7.262	6.173	7.369	4.28×10^{-6}	30.67	88.66
C28	1596	6.266	4.298	5.494	3.21×10^{-6}	30.20	88.32
						Av =	88.48 ± 0.54

However, resolution of N_2, Pu and PuN from PuN as well as Pu and PuC from carbides should be possible.

7. High Temperature Calorimetry
(A. E. Ogard)

The heat content has been determined for $U_{0.802}PU_{0.198}O_{2.00}$ and $U_{0.802}Pu_{0.198}O_{1.98}$ from 895 to 1840°C. The results are listed in Table VII and are plotted in figure 3. Also plotted in figure 3 are the heat contents of UO_2 reported previously (LA-3650-MS), and an extrapolation of the lower temperature results of G. E. Moore and K. K. Kelley on UO_2.

Table VII

Heat Content of $U_{0.802}Pu_{0.198}O_x$

H_T-H_{298}

Temp., °C	$U_{0.802}Pu_{0.198}O_{2.00}$	$U_{0.802}Pu_{0.198}O_{1.98}$
895	63.5	...
903	...	64.3
1030	73.4	73.6
1106	79.8	...
1136	...	80.6
1197	86.6	...
1220	89.0	...
1229	...	87.9
1310	95.7	96.5
1446	107.4	108.3
1547	117.8	115.7
1636	127.0	123.8
1737	136.3	135.2
1803	143.0	...
1840	...	143.3

8. Analytical Chemistry

1. The Determination of Uranium and Plutonium in Uranium-Plutonium Carbides and Nitrides
(K. Bergstresser, G. B. Nelson, G. R. Waterbury)

The measurement of U and Pu in solutions of these two elements was accomplished without prior separation by controlled-potential coulometry and potentiometric titration methods. The relative standard deviation for measuring each element was 0.3 percent for the controlled-potential coulometric method and 0.05 percent for the potentiometric titration. As an additional test of their reliability, these methods are being applied to repeated analyses of several portions from an ingot of $(U_{0.8}Pu_{0.2})C$. Data obtained to date show that the relative standard deviation of the controlled-potential coulometric measurement of U and Pu is from 0.1 to 0.2 percent and that the potentiometric titration method is not more precise than the coulometric method when carbide samples are analyzed. A statistical analysis of all of the titration results will be made when this testing is completed.

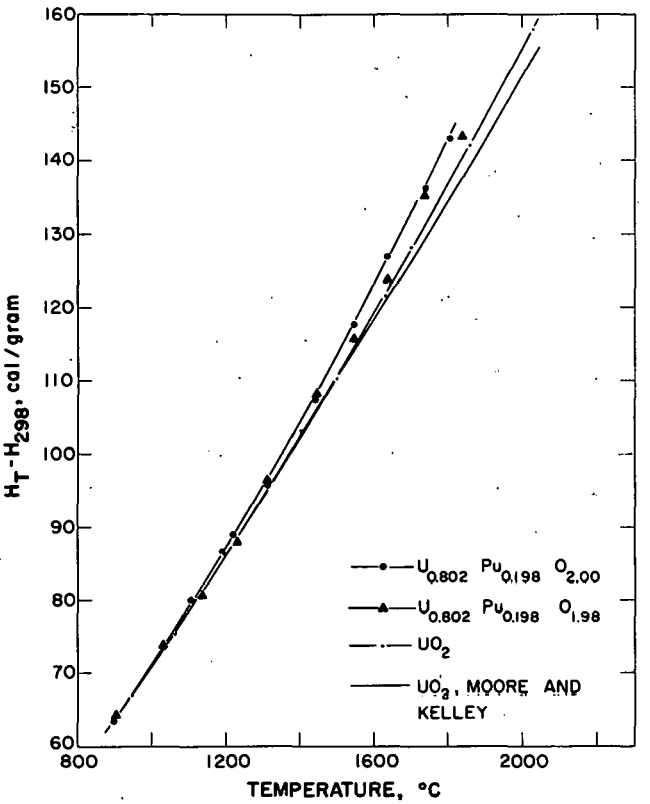

Fig. 3. Heat Contents of Uranium-Plutonium Oxides.

2. Electron Microprobe Examination of Uranium-Plutonium Carbides and Nitrides
(E. A. Hakkila, H. L. Barker)

Several specimens of $U_{0.8}Pu_{0.2}C$ from various solution treatment experiments were examined with the electron microprobe to identify inclusions and to determine the homogeneity of the materials on a microscale. Needle-like crystals and grain boundary inclusions were found to be enriched in Pu relative to the matrix material. Brown inclusions were found to contain less Pu than the surrounding matrix. Some grain boundary inclusions were enriched in C.

3. The Determination of Oxygen in Irradiated Refractory Materials (C. MacDougall, M. E. Smith)

A fused-silica furnace was designed for the inert-gas-fusion measurement of O_2 in highly radioactive materials. The assembly was tested by successfully determining O_2 in Nb, NbC, and W-Mo materials. The silicone high-vacuum grease that sealed joints in the furnace was found to deteriorate upon exposure to radiation. Following irradiation testing of several greases, the silicone grease was replaced by Fluorlube GR-362. The equipment is ready for installation in a hot cell.

4. Spectrochemical Analysis of Irradiated Uranium-Plutonium Fuels and Associated Materials (O. R. Simi)

The optical system needed to pass light from an analytical gap within the hot cell to a spectrograph outside the cell has been installed, aligned and tested. The performance of the system, transmitting 40% of the available light in the ultraviolet region, as compared to a similar source outside the cell, is considered satisfactory.

IV. REFERENCES

1. J. P. Marcon and R. Pascard, J. Inorg. Nucl. Chem. 28, 2551-60 (1966).

2. C. T. Prewitt and A. W. Sleight, Amer. Cryst. Assoc. Winter Meeting, Jan. 1967 (and private communication).

3. J. Ward, Report LA-3509 (1966).

4. D. R. Stull and G. C. Sinke, Adv. in Chem. Series No. 18, Amer. Chem. Soc. (1956).

5. D. L. Hildebrand and W. F. Hall, J. Phys. Chem. 66, 764 (1962).

6. R. Hultgren, R. L. Orr, P. D. Anderson, and K. K. Kelley, "Selected Values of Thermodynamic Properties of Metals and Alloys," J. Wiley and Sons, N. Y. (1963).

PROJECT 808

COMPATIBILITY OF SODIUM-BONDED (U,Pu)C AND (U,Pu)N FUELS WITH CLADDING MATERIALS

Person in Charge: D. B. Hall
Principal Investigators: R. H. Perkins
J. A. Leary

I. INTRODUCTION

The use of sodium for heat transfer between the fuel pellets and the cladding is desirable to lower the surface temperature of the pellets and to permit substantial tolerances in the dimensions of the pellets and the clads. The objectives of this program are to study the interactions among potential cladding materials, a sodium bond, and (U,Pu)C or (U,Pu)N, i.e., to develop the technology required for a sodium-bonded fuel element in which the fuel and cladding are compatible. The cladding materials to be studied include nickel-base alloys, high-strength austenitic stainless steels, precipitation-hardened stainless steels, and refractory metal alloys.

The compatibility of the carbide fuel with potential cladding materials will be determined as a function of the M/C ratio of the fuel. Hypo- and hyperstoichiometric mixed carbides, as well as fuel with stoichiometric composition, will be investigated. The solubility of carbon in sodium and the kinetics of carbon transfer from fuel to clad will be studied. The utilization of barriers to prevent the carburization of claddings due to carbon transport by sodium will be investigated. Considerations of compatibility and ease of preparation suggest experiments with fuel compositions of the type $(U,Pu)C_xN_yO_z$ with $x > 0.5$ and $x + y + z = 1$. These compositions will be single-phase except for a finely dispersed non-carbide phase in some cases. The Pu/U ratio in all fuels will be maintained at 0.2.

Studies of compatibility with pure mononitride fuel also will be made. The presence of a sesquinitride phase or a higher-than-usual nitrogen activity may make the fuel more nitriding and thus usually more corrosive. Hence attempts will be made to measure the nitrogen pressure from fuel preparations as well as possibly measure the evolution of other gases.

All materials going into and coming out of test will be carefully characterized, using chemical analyses, nondestructive testing, physical-property measurements, and metallography. Fuels of known composition will be produced using methods developed principally by the Ceramic Plutonium Fuel Materials Program (Project 807) at LASL. Sodium for bonding will be obtained from a hot-trapped loop with a vacuum-distillation apparatus for the determination of oxygen levels.

II. CARBIDE FUEL COMPATIBILITY STUDIES (F. B. Litton)

A. General

The objectives of this program are to study the interactions among single-phase mixed uranium-plutonium carbide, a sodium bond and potential cladding materials, i.e., to investigate the technology related to liquid-metal-bonded fuel elements. Primary emphasis will be placed on fundamental reactions occurring in the bond in $(U_{0.8}Pu_{0.2})C$-sodium-Type 316 stainless steel and $(U_{0.8}Pu_{0.2})C$-sodium-vanadium alloy. High-purity, thoroughly characterized sodium will be used for the studies. In addition, during the study, engineering information will be developed on high-strength iron- and nickel-base, precipitation-hardened, and refractory-metal

alloys in contact with sodium-bonded, single-phase mixed carbides.

B. Current Results

Materials and apparatus are being assembled to conduct the experimental program. Shake-down operation was continued on one of four isothermal sodium loops, equipped with an ANL (EB-1-26690-E) distillation assembly for oxygen analysis. The loop was cycled to, and maintained at, 750°C for extended periods without affecting the oxygen content of the sodium. The oxygen content was approximately 2 ppm. Provision was also made to obtain samples for analyzing loop sodium for additional elements, such as carbon, nitrogen, and total metallic impurities. The distillation assemblies for the three other 4 in. isothermal sodium loops were approximately 75% completed. In addition, the thermal-gradient loop was about 60% completed during this period.

An experiment was started to determine the equilibrium solubility of carbon in sodium in contact with uranium carbide in the system uranium carbide-sodium-Type 316 stainless steel. Pending arrival of uranium carbide pellets having single-phase (4.8 w/o C) and single-phase plus di-carbide (5.0 w/o C), degassed AUC-type graphite in contact with 5 g of high-purity sodium was heated in capsules of Type 316 stainless steel for 96 hr at 750°C. In order to separate the sodium bond from the graphite pellet, the capsules were inverted at the end of the heating period. Test analyses were not made during this report period.

III. SYNTHESIS AND FABRICATION OF (U,Pu)C
(M. W. Shupe, A. E. Ogard, J. A. Leary)

A. General

Development of procedures for standardizing the process used to prepare carbide fuel pellets is being continued. Basic process steps are (1) multiple arc melting of U, Pu, and C, (2) crushing and grinding to -325 mesh powder, (3) cold pressing to a 0.284-in.-diameter pellet that is ∿ 69% of theoretical density, and (4) sintering at 1700°C in Ar. Powder handling steps 2 and 3 are conducted in an inert atmosphere enclosure having impurity levels of $\leq$ 4 ppm oxygen and $\leq$ 4 ppm oxygen and $\leq$ 0.5 ppm water. Ingots and pellets from steps 1 and 4 are handled in flowing Ar of lesser purity.

B. Current Results

Five additional development lots were prepared and evaluated during this period. Sound pellets that could be handled without damage were produced in all cases. As shown in Table I, within a given

Table I

Results of Five Development Lots of $U_{0.80}Pu_{0.20}C$

Lot No.	No. Pellets	Av Diam (in.)	No. Pellets Outside of Spec.	Sintered Density, % Theo.
5-39-1	14	0.262	0	89
5-41-2	14	0.260	0	90
5-63-1	9	0.263	0	90
5-63-2	13	0.267	1	88
5-67-1	7	0.267	1	88

lot the pellet diameter could be controlled to within the specified tolerance (± 0.002 in.) for pellets in the specification density range. Pellets from lot 5-39-1 were single phase except for the outer 0.001 in. which contained the characteristic microstructure. This was attributed mainly to graphite components in the sintering furnace. After minor adjustments in process equipment and procedure, pellets produced in later lots (5-63-1, 5-63-2, and 5-67-1) were single-phase monocarbide by metallographic and by x-ray diffraction analysis. Variation of Pu/U ratio was less than 1%.

Current effort is being devoted to minimizing lot-to-lot variations, and to increasing the number of pellets produced in each lot.

IV. NITRIDE FUEL STUDIES
(B. J. Thamer)

A. General

The studies on nitride fuels have been allocated less manpower and materials than those on carbide fuels. However, the preparations for the testing of compatibility have proceeded as well as possible without nitride pellets. The available literature has been reviewed in a report.[1] The literature shows that the pickup of water vapor or oxygen by the nitride fuel can convert some of the mononitride to uranium sesquinitride which is more strongly nitriding toward the clad[2,3,4] and usually less compatible with it. The sesquinitride's decomposition produces an appreciable nitrogen pressure at only moderate temperatures:

$$2\ U_2N_3(s) = 4\ UN(s) + N_2(g).$$

The measurements of Bugl and Bauer indicate this pressure to be 1 mm Hg at slightly less than 900°C.[5]

B. Current Results

An apparatus has been built to measure the nitrogen pressure of a fuel material upon heating. The apparatus is made principally of Type 304 stainless steel except for the heated area which is quartz. Nitride materials to test should be available within the next quarter. Compositional analyses of the evolved gases will also be made in order to detect gases other than nitrogen.

V. LOADING FACILITY FOR TEST CAPSULES (D. N. Dunning)

A. General

A complete system for loading ceramic fuel pellets and sodium into test capsules is now being assembled. The basic approach is to supply sodium of known and controllable quality to capsules containing (U,Pu)C fuel pellets. The evacuable gloveboxes are to be provided with systems for gas cleanup as well as evacuation equipment for the control of impurities prior to final welds. Figure 1 is a

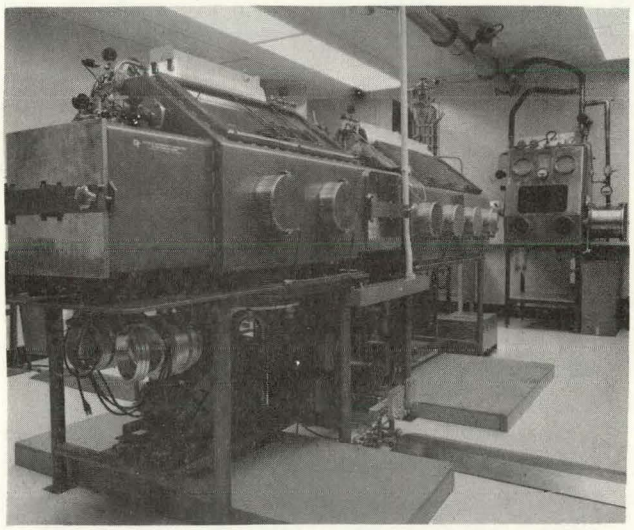

Fig. 1. Facility for the Fuel Pellet Loading, Sodium Bonding, and Final Welding of Test Capsules.

general laboratory view showing the welding box, sodium loading box, and fuel loading box.

B. Current Results

The components of the system and their status are as follows:

1. Fuel-Loading Station

The inert-atmosphere glovebox for this work is completed except for the loading-flange area. Parts for this area are being fabricated. The loading approach provides for loading the (Pu,U)C pellets from an alpha-hot box into a capsule such that the outside of the capsule is maintained free of contamination. An inner sleeve, made of aluminum, is discarded after each loading operation as a control on contamination.

2. Sodium-Purification Loop and Sodium-Loading Box

The sodium-purification loop serves as the source of the bonding sodium. This loop has been designed and completely fabricated. Figure 2 is a

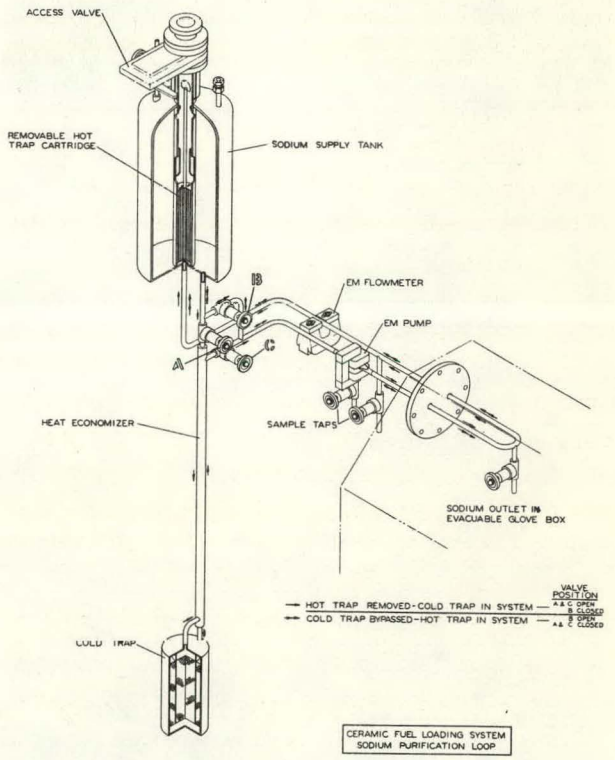

Fig. 2. Sodium-Purification Loop.

schematic drawing of the essential parts of the loop. There are several operational modes that can be used with this system; hot-trapped sodium can be isolated for insertion into the capsules, or the hot trap can be removed and cold-trapped sodium can be isolated for capsule loading. For sodium of controlled impurity, the hot trap is removed and known impurities such as oxygen are added through the

access valve. Solubility levels are then controlled by the cold trap temperature. One sample tap is permanently connected to the vacuum-distillation equipment for analysis prior to box entry. Figure 3

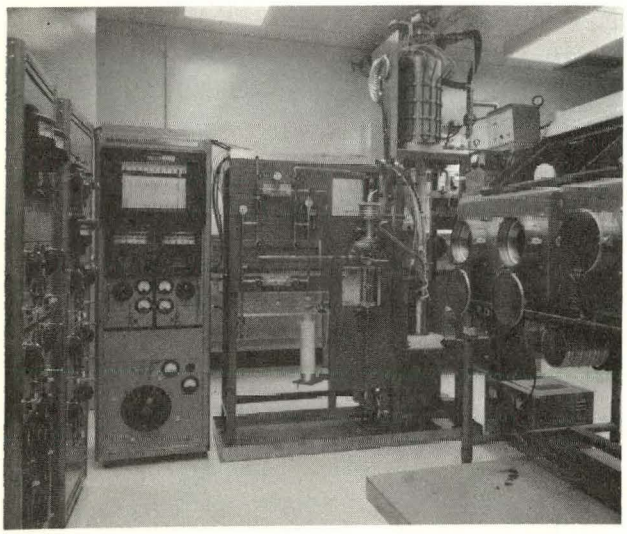

Fig. 3. Sodium-Supply Loop, Sodium-Loading Glovebox and Vacuum-Distillation Equipment.

shows the sodium-supply loop, sodium-loading box, vacuum distillation equipment and associated controls.

Two different approaches are being taken for the loading of the sodium into the capsules. One of these is the solid-sodium loading approach. In this approach the sodium is brought into the box at a controlled temperature and cast into an extrusion cylinder. Figure 4 is a photograph of this equipment. Temperature profiles are being run prior to

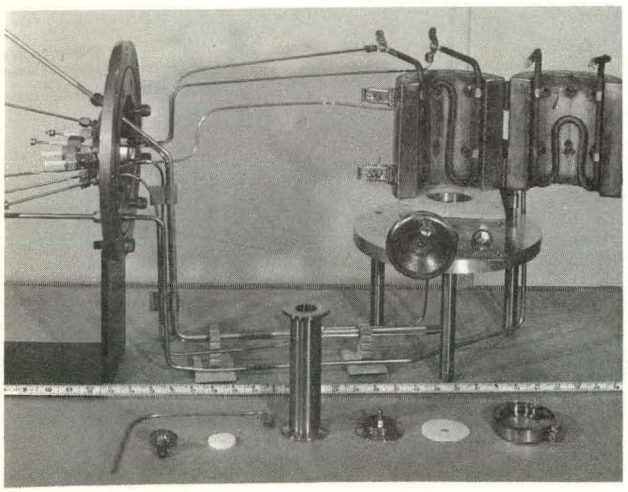

Fig. 4. Sodium-Casting Furnace.

minimizing thermal gradients. The extrusion equipment has been designed, fabricated, and installed in the box except for the hot wire cut-off and run-out guides. The other loading approach is to use a device for liquid metering and loading. This system has a positive-displacement bellows for the loading and a continuous circulation of sodium during stand-by. This equipment is in final design.

The sodium-loading box is being equipped to operate with either an evacuation and back-fill with an inert atmosphere or with recirculating gas. The evacuation equipment is connected to the exhaust system for plutonium in case a spill should occur. The purification equipment for recirculating inert gas is being purchased to maintain the 50-cu-ft volume at less than 10 ppm (oxygen plus moisture) with two glove ports open.

3. Welding Box

The welding box is complete. The capsules will receive the final closure in this box.

4. Sodium-Bonding Equipment

Revisions have been made in the initial approach to establish the sodium bond between the fuel and the cladding. Present plans call for establishing the bond by placing the loaded and welded capsule on a magneto-strictive device at temperatures above the wetting temperatures. The capsule is then put into a centrifuge to seat the fuel pellets in the bottom of the capsule while the sodium solidifies. The furnace and controls have been assembled and the magneto-strictive device is on order.

VI. POST-TEST EXAMINATION
(J. H. Bender)

A. General

Metallographic examination is one of the primary methods for evaluating the compatibility of fuels with cladding. Metallographic techniques for (U,Pu)C and (U,Pu)N of varying compositions are therefore being developed and standardized. A similar approach will be taken with cladding materials. This should insure that any changes in the clad and fuel structures during tests of compatibility can be properly identified and evaluated.

B. Current Results

The metallographic technique for the characterization of uranium, plutonium carbide has been developed further. The following preparative steps

were used to obtain the microstructures of Figs. 5-8.

Samples were vacuum-mounted in epoxy resin and ground successively with 180, 240, 320, and 600 grit SiC papers lubricated with lapping oil. They were rough-polished for 10 min with 15 μ diamond paste on "Texmet" followed by 45 min with 6 μ diamond on "Texmet" and 30 min with 1 μ diamond on "Texmet". The 6 μ and 1 μ polish used an automatic polishing attachment ("Whirlimet"). The lubricant for all polishing steps was silicone oil (Dow Corning #200 fluid). The final polish was for 30 min with 0.05 μ Al_2O_3 on "Microcloth" and silicone-oil lubricant using a vibratory polisher ("Vibromet"). The specimens were stain-etched electrolytically with 1:1:1 nitric, acetic, and lactic acids for 10 sec at 2.5 vdc.

Figure 5 is typical of the structure observed

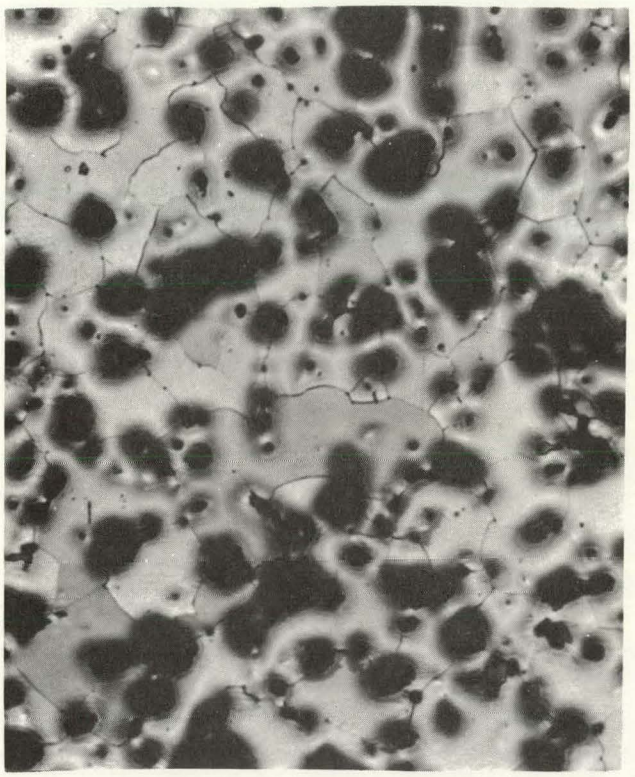

Fig. 5. Stoichiometric (U,Pu)C. Matrix = MC. Etched, 300X (not reduced).

in a stoichiometric sample of (U,Pu)C. No metal (M) or sesquicarbide (M_2C_3) phase is evident in the grain boundaries and only occasionally is the sesquicarbide phase noted as a dispersed phase within a grain. (Here and subsequently the large dark areas are pores.)

Figure 6 exhibits the structure present in a hyperstoichiometric sample. The sesquicarbide phase is evident in grain boundaries and within grains in conjunction with the dicarbide phase (MC_2).

Fig. 6. Hyperstoichiometric (U,Pu)C. Matrix = MC, White Phase = M_2C_3, Needle Phase = MC_2. Etched, 300X (not reduced).

Figure 7 is typical of the structure observed in a hypostoichiometric sample. The free metal phase is seen in grain boundaries, within grains, and in the pores of the sintered body.

Electron microscopy of stain-etched specimens by replication methods is not feasible because of the oxide film on the sample surface. To alleviate this condition and permit replication, it was found that swabbing the (U,Pu)C samples with the electrolyte at a zero potential removed the oxide film.

A further investigation of the swabbing technique is in progress to aid in the metallographic analysis of metal versus sesquicarbide phases by electron microscopy.

Figure 8 shows the hypostoichiometric sample after swabbing at a zero potential. Grain boundaries and the free metal phase are still evident in the structure after the removal of the oxide film.

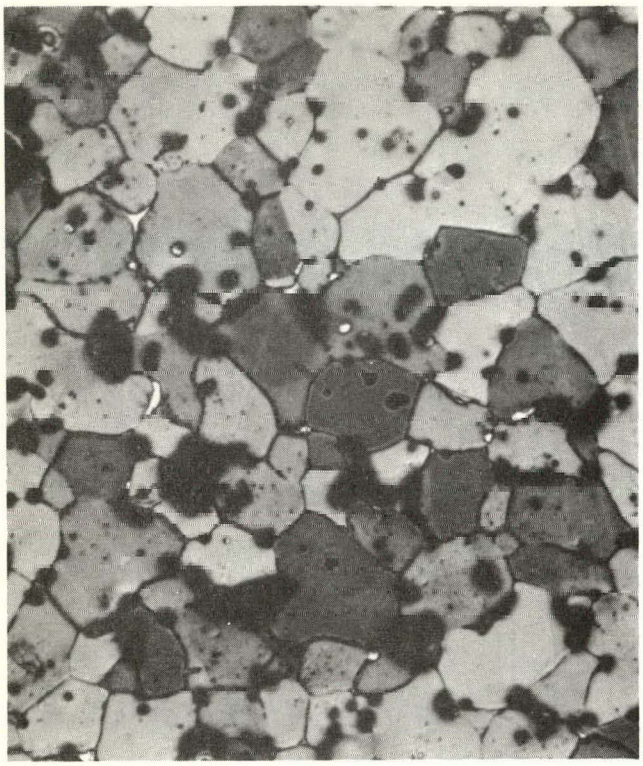

Fig. 7. Hypostoichiometric (U,Pu)C. Matrix = MC, White Phase = M. Etched, 300X (not reduced).

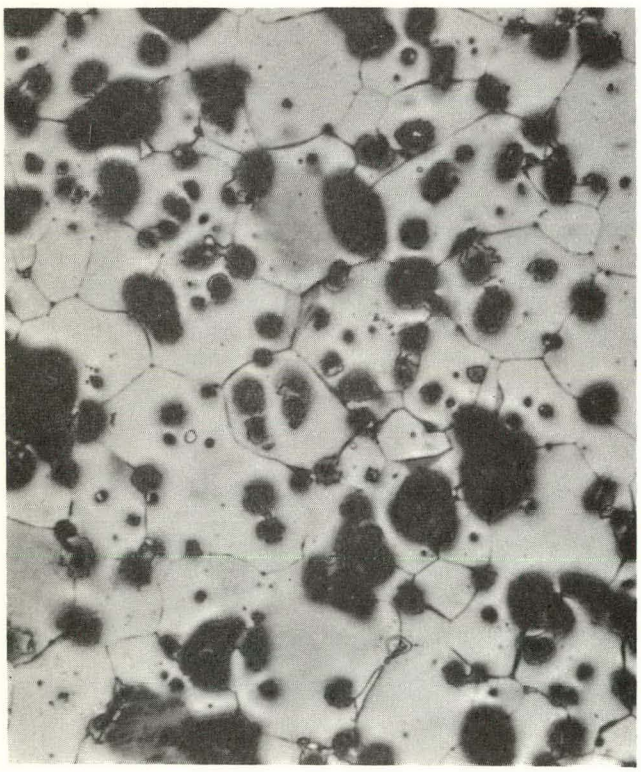

Fig. 8. Hypostoichiometric (U,Pu)C. Etched, Swabbed, 300X (not reduced).

VII. EBR-II IRRADIATIONS

(J. O. Barner, R. L. Cubitt, G. L. Ragan)

A. General

The purpose of this sub-program is to evaluate, from an irradiation standpoint, candidate fuel-pin systems for the LMFBR program. A fuel-pin system of the following type is the reference design: pellets of single-phase (U,Pu)C are separated by a sodium gap from a cladding of a precipitation-hardened alloy or other high-temperature alloy. Seven fuel-element tests are planned in the initial group of a continuing series of EBR-II irradiation experiments.

B. Current Results

An approval in principle has been received from Argonne National Laboratory for the irradiation of seven capsules in EBR-II. The irradiations are to commence in the latter part of calendar 1967. The capsules are to be irradiated under the following conditions:

1. Lineal power: 29.15 to 30.20 kW/ft (max).
2. Fuel composition: $(U_{0.8}Pu_{0.2})C$ (single-phase, fully enriched, sintered).
3. Fuel density: 85% and 90% of theoretical.
4. Smear density: 75% and 80%.
5. Clad size: 0.300 in. o.d. x 0.010 in. wall.
6. Fuel size: 0.265 in. o.d. x 0.250 in. high.
7. Clad type: 316 SS and Hastelloy-X.
8. Maximum clad temperature: 1250°F.
9. Maximum fuel centerline temperature: 2230°F.
10. Burnup: 1/4 to 3/4 g fissioned per cm^3.

The hazards report for these capsules is 95% complete. The drawings, design of the shipping containers, and evaluation of non-destructuve testing procedures remain to be completed for inclusion in the hazards report.

The Omega West Reactor is being considered for preliminary irradiation of sodium-bonded mixed-carbide fuels. The OWREX environmental cells,[6] still present in the OWR vessel, can accommodate clad fuel specimens of the proposed diameter and can remove the heat from fuel test lengths up to 4 in.

A series of neutronic calculations was run to determine the linear power levels and radial power profiles attainable for various fuels. The calculations were made with the one-dimensional transport code DTF-IV,[7] representing the OWR as an infinitely long cylinder, with the environmental cell and

contained fuel rod also infinitely long cylinders, centered in the core. Unshielded (σ_s per atom = ∞) Hansen-Roach 16-group cross sections were used.[8]

Similar calculations were run in 1963 for the liquid plutonium fuels that were subsequently tested. The absolute values of powers obtained in the present calculations were normalized by using the factor required to fit the 1963 calculations to the experimentally observed values. Experience has shown (e.g., Fig. 8 of Ref. 6) that both the absolute value and radial variation of power are well represented by such normalized calculations.

The results of the recent calculations are summarized in Table II. Problem No. 1184 corresponds to the reference fuel (uranium content fully enriched) proposed for irradiation in EBR-II, while No. 1185 corresponds to the breeder fuel (uranium content depleted). The reduced density cases are of interest in connection with a fission product releasing fuel and to help raise the central fuel temperature. Assuming the conductivity to be proportional to the carbide density, the last column of the table gives estimates of the temperature difference between center and edge of the fuel, relative to that of the reference case. These temperature estimates are based on the further assumption that the temperature difference is proportional to the heat generated in the inner zone (0.219-in. diam) of the problem. Spot checks with exact calculations indicate this approximation to be reasonable.

The variation of power density with radius is shown, for two selected cases, in Fig. 9. The fissile content of the fuel is essentially the same for the two problems. The average powers generated are almost the same, but the power profiles are markedly different. Preliminary investigation indicates that the difference is largely attributable to the large resonance in ^{239}Pu cross sections at 0.3 eV. (Peak values are about five times the thermal values.)

Table II

CALCULATED CONDITIONS FOR CARBIDES IN OWREX

Pin Diameter = 0.265 in., OWR at 8 MW

Fuel Composition					Power				
Prob. No.	%TD:100	$N_{Pu}:N_{HA}$	$N_{235}:N_U$	Relative $N_{fissile}$	Linear kW/ft	Average MW/liter	Center:Av	Edge:Av	Relative Index of Temperature
Ref.	0.9	0.20	0.93	1.00	30.0	2.76	1.00	1.00	1.00
1184	0.9	0.20	0.93	1.00	35.9	3.30	0.33	4.10	0.56
1185	0.9	0.20	0.00	0.20	22.2	2.04	0.40	2.39	0.47
1188	0.9	0.00	0.20	0.21	22.7	2.08	0.68	1.54	0.60
1186	0.9	0.00	0.93	1.00	38.5	3.54	0.40	3.31	0.71
1193	0.8	0.00	0.93	0.89	37.2	3.42	0.40	3.08	0.80
1194	0.7	0.00	0.93	0.78	35.9	3.30	0.41	2.83	0.91
1187	0.9	0.00	0.50	0.54	31.2	2.87	0.45	2.34	0.68
1190	0.8	0.00	0.56	0.54	31.4	2.89	0.45	2.33	0.77
1191	0.7	0.00	0.64	0.54	31.6	2.91	0.46	2.31	0.89

NOTES:

Reference Problem is the Project 808 reference proposal.

TD = theoretical density of the carbide fuel
N = atom density
HA = heavy atoms

Relative $N_{fissile}$ is total fissile atom density relative to the reference case.

Relative Index of Temperature is the ratio of the approximate center-to-edge temperature difference to that of the reference case.

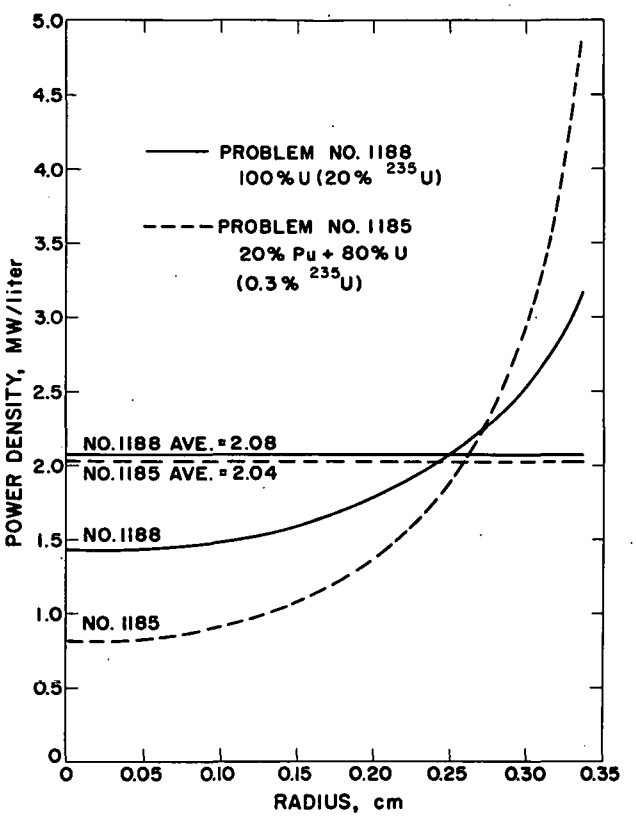

Fig. 9. Variation of Power Density with Radius for Mixed Monocarbide Fuels at 90% of Theoretical Density.

References

1. B. J. Thamer, "The Use of (U,Pu)N Fuel with a Sodium Bond: A Summary of Existing Data," Report LA-3646, Los Alamos Scientific Laboratory, March 27, 1967.
2. D. E. Price et al., "The Compatibility of Uranium Nitride with Potential Cladding Materials," Report BMI-1760, Battelle Memorial Institute, Feb. 8, 1966.
3. E. J. McIver et al., "The Oxidation and Ignition of UN and UC, Part II. Single Crystal Oxidation Studies," Report AERE-R-4985, Atomic Energy Research Establishment, Harwell, Sept., 1965.
4. R. M. Dell et al., "The Hydrolysis of Uranium Mononitride," Report AERE-R-4984, Atomic Energy Research Establishment, Harwell, Nov., 1965.
5. J. Bugl and A. A. Bauer, "Phase, Thermodynamic, Oxidation, and Corrosion Studies of the System Uranium-Nitrogen," Report BMI-1692, Battelle Memorial Institute, Sept. 4, 1964.
6. R. L. Cubitt, G. L. Ragan, and D. C. Kirkpatrick, "The Irradiation of Liquid Plutonium Fuels in a Thermal Reactor," Report LA-3557-MS, Los Alamos Scientific Laboratory (1966).
7. K. D. Lathrop, "DTF-IV, a FORTRAN-IV Program for Solving the Multigroup Transport Equation with Anisotropic Scattering," Report LA-3373, Los Alamos Scientific Laboratory (1965).
8. "Los Alamos Group-Averaged Cross Sections," L. D. Connolly, ed., Report LAMS-2941, Los Alamos Scientific Laboratory (1963).

PROJECT 811

REACTOR NUCLEAR ANALYSIS METHODS AND CONCEPT EVALUATIONS

Person in Charge: D. B. Hall
Principal Investigator: G. H. Best

I. INTRODUCTION

The primary objective of this project is to continue the development of numerical methods for the treatment of neutron and gamma-ray transport problems. Current work in this area includes the application of continuous analytic continuation to reactor kinetics problems (Section II) and the study of heat deposition in fast reactor shields (Section III). The secondary objective is the development of techniques for advanced concept evaluation and the evaluation of selected concepts. Current work in this area is reported in Section IV.

II. APPLICATION OF CONTINUOUS ANALYTIC CONTINUATION TO REACTOR KINETIC PROBLEMS
(J. C. Vigil, B. M. Carmichael)

A. General

The ANCON code,[1] which is based on the continuous analytic continuation method for solving reactor kinetics equations, provides a calculational technique in which the successive time steps in the problem are automatically adjusted to be consistent with the rate of change of neutron population, and with satisfying preselected error criteria for the entire problem. This calculational procedure is as much as 25 times faster than the RTS code[2] for fast reactor excursions. For slow excursions, the code selects the best time step on the basis of delayed neutron precursor population, rather than on the basis of the neutron population itself.

B. Current Results

Programming work on the unified ANCON code package has been completed. The ANCON code solves the point reactor kinetics equations in the form

$$\frac{dn(t)}{dt} = \frac{1}{\Lambda}\,[\rho(t) - \beta]\, n(t) + \sum_{i=1}^{I} \lambda_i\, c_i(t) + S \qquad (1)$$

$$\frac{dc_i(t)}{dt} = \frac{\beta_i}{\Lambda}\, n(t) - \lambda_i\, c_i(t) \qquad (i = 1, \ldots, I) \qquad (2)$$

$$\rho(t) = I(t) + F(t). \qquad (3)$$

Three options are available for the impressed reactivity I(t). They are

$$I(t) = \rho_o \sin \omega t \qquad (4a)$$

$$I(t) = \sum_{\ell=0}^{L} a_\ell\, t^\ell \qquad (4b)$$

$$\left.\begin{aligned} I(t) &= \sum_{\ell=0}^{L} a_\ell\, t^\ell && (0 \le t < t_1) \\ I(t) &= \sum_{\ell=0}^{L} a_\ell\, t_1^\ell + \sum_{m=0}^{M} b_m (t - t_1)^m && (t_1 \le t < t_2) \\ I(t) &= \sum_{\ell=0}^{L} a_\ell\, t_1^\ell + \sum_{m=0}^{M} b_m (t_2 - t_1)^m && (t \ge t_2) \end{aligned}\right\} \qquad (4c)$$

The first option (Eq. 4a) represents a sinusoidal input of reactivity. Equation 4b can be used to represent the reactivity variation due to movement of a central rod or any other input of reactivity which can be represented by a polynomial in t. The third option (Eq. 4c) can be used to simulate rod withdrawal in the interval $0 \le t < t_1$ followed by a scram in the interval $t_1 \le t < t_2$. Either of the polynomials in Eq. 4c can be omitted if desired.

The function F(t) represents the inherent reactivity feedback. Two options are available:

$$F(t) = \sum_{j=1}^{J} \sum_{k=1}^{K_j} \alpha_{jk} [T_j(t) - T_j(0)]^k \qquad (5a)$$

and

$$F(t) = \sum_{j=1}^{J} \alpha_j [T_j(t) - T_j(0)]^{\chi_j} \qquad (0 < \chi_j < 1) \quad . \qquad (5b)$$

In the first option (Eq. 5a), the feedback is represented in terms of a polynomial in the temperature T for each lump j. This form is useful for thermal base reactivity feedback. The second option (Eq. 5b) represents the feedback in terms of a constant coefficient α_j multiplied by the χ_jth power of the temperature for each lump j. This form is useful for Doppler reactivity feedback.

Three options are available for the lump-type thermodynamic equations which are used in conjunction with Eqs. 5. These options are:

$$C_j(t) \frac{dT_j(t)}{dt} = Q_j P(t) - a_j \qquad (j = 1, \ldots, J) \qquad (6a)$$

$$C_j(t) \frac{dT_j(t)}{dt} = Q_j P(t) - a_j T_j(t) \qquad (6b)$$

$$C_j(t) \frac{dT_j(t)}{dt} = Q_j P(t) - \sum_{k=1}^{J} h_c^{j \to k} [T_j(t) - T_k(t)] - \sum_{k=1}^{J} h_r^{j \to k} [T_j^4(t) - T_k^4(t)] \quad . \qquad (6c)$$

Equation 6a represents constant heat loss from lump j while Eq. 6b represents heat removal proportional to T_j. Equation 6c represents heat loss from lump j to other lumps by conduction, convection, or radiation. Either the term involving h_c or that involving h_r may be omitted if desired.

The heat capacity $C_j(t)$ for lump j is represented in terms of a polynomial in T_j:

$$C_j(t) = \sum_{k=0}^{K_j} \gamma_{jk} [T_j(t) - T_j(0)]^k \quad . \qquad (7)$$

If the heat capacity for lump j is a constant, then $K_j = 0$.

The variable in Eqs. 6 may be used, in some cases, to represent variables other than temperature. For example, T_j in Eq. 6b may be used to represent the void volume fraction in lump j if $C_j(t) = 1$. In any case, the code is programmed so that lump-type thermodynamic equations other than Eqs. 6 can be added without requiring a modification of the main program.

III. HEAT DEPOSITION IN FAST REACTOR SHIELDS
(M. E. Battat and D. J. Dudziak)

For studies of heat deposition in fast reactor shields, a comparison has been made between data for fission product decay from ^{239}Pu fast fission, using the FPIC code,[3] and experimental data of Johnston.[4] Anderson's fission product yields[5] for fast fission of ^{239}Pu were used in the FPIC code. Both beta and gamma energy release rates were calculated for decay times varying from 50 to 175 days, following either an instantaneous fission burst or 10 days constant power operation. The calculated individual beta and gamma contributions differed by as much as a factor of two from the experimental values, but the calculated total energy release was only slightly less than Johnston's experimental values.

IV. ADVANCED SYSTEM TECHNICAL EVALUATIONS
(J. J. Prabulos, Jr. and W. H. Hannum)

A. General

A variety of general reactor problems -- coolant voiding effects, attainable breeding ratios, fuel vs poison control have been considered for certain reactor concepts. Current results of worth in some of the above categories are summarized in the following sections.

B. Sodium Void Effects in the Liquid Plutonium Modular Reactor

Sodium void eigenvalue calculations have been carried out with the DTF-BURN code[6] for a modular version of the Los Alamos liquid plutonium fast breeder reactor for complete voiding of the core and complete voiding of the blanket. The results are given in Table I for the reactor configurations at the beginning-, middle-, and end-of-life. The coefficients are all negative initially, and most values become smaller with time. With a reflective outer boundary condition, however, the coefficient for complete voiding of the blanket changes from negative to positive near the middle-of-life.

TABLE I

SODIUM VOID COEFFICIENTS
LOS ALAMOS MODULAR LIQUID PLUTONIUM FAST BREEDER REACTOR

Void Coefficient - %Δk

	Vacuum Boundary Condition		Reflective Boundary Condition	
Time	Complete Core Voiding	Complete Blanket Voiding	Complete Core Voiding	Complete Blanket Voiding
Beginning-of-Life	-1.0	-0.4	-0.9	-0.04
240 Days Middle-of-Life	-0.7	-0.2	-0.5	+0.3
480 Days End-of-Life	-0.3	-0.2	-0.05	+0.8

For comparison, sodium void eigenvalue calculations were also run for the Westinghouse modular fast breeder reactor[7] with poison control. The results for this reactor design are listed in Table II.

TABLE II

SODIUM VOID COEFFICIENTS
WESTINGHOUSE MODULAR FAST BREEDER REACTOR

Void Coefficient - %Δk

	Vacuum Boundary Condition		Reflective Boundary Condition	
Time	Complete Core Voiding	Complete Blanket Voiding	Complete Core Voiding	Complete Blanket Voiding
Beginning-of-Life	+1.8	-0.1	+2.0	-0.03
400 Days Middle-of-Life	+1.6	-0.2	+2.0	+0.04
1098 Days End-of-Life	+1.4	-0.2	+2.4	+0.2

Each of the values for complete core voiding is positive and larger in absolute value than the corresponding one for the liquid plutonium design. Values and trends for complete blanket voiding, however, are generally similar to those given in Table I. A comparison of values for the two reactor designs thus indicates the superiority of the liquid plutonium reactor with respect to sodium voiding effects.

C. Effects of Different Control Methods in the Liquid Plutonium Modular Reactor

In order to assess the difference between alternative control methods in the liquid plutonium reactor, some DTF-BURN depletion calculations for single modules with tantalum poison control were run for different core radii. All designs analyzed with poison control had the same initial regional compositions and the same module size as the analysis of the design with moving fuel control reported in last quarter's report.[8]

First, the radius necessary to accommodate an average core burnup of 1 gf/cc with control poison was estimated. The radius chosen was 27.5 cm, and selected design parameters are listed in Table III as a function of time. The results indicate that the core radius selected was not quite large enough to accommodate an average burnup of 1 gf/cc. The low initial values of the breeding ratio are due to the excessive amounts of control poison required to hold down the excess reactivity at the beginning-of-life. A comparison of these values with the corresponding ones for the design with moving fuel control indicates the potential advantages of moving-fuel control. If poison rods are used, fuel management and further design refinements are necessary to eliminate the excessive number of absorptions in control poison with concomitant lowering of the breeding gain.

In order to evaluate the effect of increasing the core radius in poison-controlled modules, selected design parameters as a function of core radius are listed in Table IV for various times. Results given in the table are all for modules with a vacuum boundary condition at the outer edge.

Breeding ratios are higher for the smaller core radii. Consequently, a design with a smaller radius would probably be required in order to obtain acceptable breeding gains in a poison-controlled system. Since a smaller core radius will not tolerate as high a burnup as a larger one, fuel management and further design refinements are indicated.

D. Miscellaneous Calculational Studies for the Westinghouse Modular Fast Breeder Reactor

Breeding ratio values obtained from DTF-BURN transport and SIZZLE[9] diffusion burnup calculations were compared as a function of time. Little difference was observed between the two sets of values, indicating the adequacy of the diffusion theory for this system.

The effect of splitting the blanket into two regions was studied in point depletion calculations for the system. Computations were run for a 1-region, 15-interval blanket and for a 2-region blanket (8-interval and 7-interval regions). The reactivity difference resulting from the use of the split blanket was found to be negligible by comparing

TABLE III

LIQUID PLUTONIUM MODULAR FAST BREEDER REACTOR
(POISON CONTROL)

Selected Design Parameters as a Function of Time

Core Radius = 2.75 cm

Time (days)	Breeding Ratio	Core Power Fraction	Core Peak to Average Power	Blanket Peak to Average Power	Fraction Neutrons Fission Product	Core FP Density x 10^{-21} Atoms/cc	Poison Density x 10^{-24} Atoms/cc
A. Vacuum Boundary Condition (Outer Edge)							
0.0	0.735	0.8302	1.525	3.809	0.0020	0.000	0.029
18.5	0.748	0.8262	1.515	3.809	0.0024	0.031	0.028
60.0	0.778	0.8160	1.495	3.795	0.0034	0.101	0.025
120.0	0.824	0.7998	1.462	3.773	0.0049	0.200	0.022
240.0	0.920	0.7637	1.393	3.732	0.0081	0.390	0.015
360.0	1.019	0.7224	1.320	3.694	0.0115	0.572	0.009
480.0	1.116	0.6768	1.245	3.659	0.0152	0.743	0.002
560.0	1.177	0.6446	1.195	3.639	0.0178	0.852	-0.001
B. Reflective Boundary Condition (Outer Edge)							
0.0	0.911	0.8013	1.521	3.158	0.0025	0.000	0.029
18.5	0.928	0.7958	1.510	3.147	0.0030	0.030	0.028
60.0	0.964	0.7831	1.491	3.116	0.0040	0.097	0.026
120.0	1.019	0.7626	1.459	3.066	0.0054	0.192	0.023
240.0	1.128	0.7193	1.396	2.974	0.0084	0.374	0.017
360.0	1.234	0.6709	1.332	2.875	0.0116	0.546	0.011
480.0	1.330	0.6195	1.271	2.772	0.0148	0.706	0.006
560.0	1.384	0.5844	1.233	2.700	0.0170	0.805	0.003

TABLE IV

LIQUID PLUTONIUM MODULAR FAST BREEDER REACTOR
(POISON CONTROL AND VACUUM BOUNDARY CONDITION)

Selected Design Parameters as a Function of Core Radius

Core Radius (cm)	Breeding Ratio	Core Power Fraction	Core Peak to Average Power	Blanket Peak to Average Power	Poison Density x 10^{-24} Atoms/cc	Fraction Neutrons Control Poison	Total Leakage
A. Zero Days							
28.5	0.681	0.8431	1.553	3.687	0.031	0.2722	0.0536
27.5	0.735	0.8302	1.525	3.809	0.029	0.2519	0.0547
23.0	1.059	0.7505	1.352	4.536	0.015	0.1275	0.0623
B. 60 Days							
28.5	0.719	0.8306	1.526	3.671	0.028	0.2514	0.0571
27.5	0.778	0.8160	1.495	3.795	0.025	0.2291	0.0584
23.0	1.133	0.7235	1.303	4.517	0.010	0.0890	0.0677
C. 120 Days							
28.5	0.760	0.8163	1.497	3.651	0.024	0.2288	0.0610
27.5	0.824	0.7998	1.462	3.773	0.022	0.2039	0.0626
23.0	1.206	0.6937	1.250	4.496	0.005	0.0478	0.0735
D. 240 Days							
28.5	0.847	0.7847	1.434	3.612	0.018	0.1801	0.0694
27.5	0.920	0.7637	1.393	3.732	0.015	0.1501	0.0717

critical tantalum core poison densities as a function of time for the split and single blanket calculations. Final nuclide masses from the split and single blanket calculations were also compared for the various blanket nuclides. Significant differences were noted only for the higher plutonium isotopes in the chain, which are, however, present only in small amounts. Thus, a single-region blanket calculation is probably adequate, unless a precise knowledge of higher plutonium isotope densities is required.

The SIZZLE diffusion burnup program has two options for computing the macroscopic diffusion coefficient used in the solution of the multigroup diffusion equation. With the first option designed for systems where scattering is primarily isotropic, the diffusion coefficient is computed from the formula

$$D = (1/3\ \Sigma_{tr}) \quad .$$

With the alternative option for systems with anisotropic scattering, the diffusion coefficient is calculated from the formula

$$D = (1/3\ \Sigma_{tr})\left(1 - 0.4\ \frac{\Sigma_a}{\Sigma_{tr}}\right)^{-2} \quad .$$

Calculations were run for both options for single modules with a vacuum boundary condition at the outer edge. A comparison of critical core tantalum poison densities as a function of time for the two options showed little difference in reactivity. A comparison of nuclide masses showed almost no difference between the two options for the core nuclides. Blanket effects, while larger than those for the core, were also small, showing that anisotropic scattering effects are relatively unimportant in the Westinghouse design.

E. Depletion Calculation Comparisons for Liquid Plutonium Modular Reactor

Comparable 15-group depletion calculations were run with DTF-BURN and SIZZLE. A comparison of critical core tantalum poison densities obtained with the two programs showed the necessity of using transport theory for an accurate estimate of the reactivity of this system. A comparison of nuclide masses showed significant differences in the results obtained for ^{241}Pu and ^{242}Pu in the core and for ^{236}U, ^{239}Np, ^{241}Pu and ^{242}Pu in the blanket.

Region and point depletion calculations run with the DTF-BURN code were also compared for the system. No difference was observed in the masses calculated for the core nuclides, because the flux distribution was relatively flat across the region. For the blanket of the module, however, considerable difference existed between the two options in the masses calculated for ^{241}Pu and ^{242}Pu; these differences were greater for modules with a vacuum boundary condition at the outer edge than for those with a reflective one. No difference was observed in the critical core tantalum poison densities as a function of time in the calculations using the point and region options for the determination of nuclide concentration changes. This is because ^{241}Pu and ^{242}Pu, for which differences were calculated, are present only in minute amounts and do not have any significant effect on the system reactivity.

F. Effect of Different Methods of Calculated $\bar{\nu}$ on Nuclide Masses Computed with the DTF-BURN Code

In DTF-BURN, the factor $\bar{\nu}$ is used in the solution of the burnup differential equations. In an early version of the program, $\bar{\nu}$ was calculated from the expression

$$\bar{\nu} = \frac{\int_{reactor} \sum_{j=1}^{IGM} (\nu\ \Sigma_f)^j\ dV}{\int_{reactor} \sum_{j=1}^{IGM} (\Sigma_f)^j\ dV} \quad .$$

However, the program was subsequently revised so that $\bar{\nu}$ is computed by flux-averaging,

$$\bar{\nu} = \frac{\int_{reactor} \sum_{j=1}^{IGM} \phi^j (\nu\ \Sigma_f)^j\ dV}{\int_{reactor} \sum_{j=1}^{IGM} \phi^j (\Sigma_f)^j\ dV} \quad .$$

Comparative calculations were performed for a liquid plutonium module with both subroutines in order to determine the effects of the revision on the computation of nuclide masses. The effect on the nuclide masses computed was negligible.

References

1. J. C. Vigil, "Solution of the Nonlinear Reactor Kinetics Equations by Continuous Analytic Continuation," Report LA-3518, Los Alamos Scientific Laboratory (1966).

2. G. R. Keepin and C. W. Cox, Nucl. Sci. Eng. 8, 670 (1960).

3. K. O. Koebberling, W. E. Drull, and J. H. Wilson, "Lockheed Fission Product Inventory Code," Report ER-6906, Lockheed Georgia Company (1964).

4. K. Johnston, J. Nucl. Energy 19, 527 (1965).

5. C. A. Anderson, Jr., "Fission Product Yields from Fast (1 MeV) Neutron Fission of Pu-239," Report LA-3383, Los Alamos Scientific Laboratory (1965).

6. J. J. Prabulos, Jr., "DTF-BURN, a Multigroup Transport Theory Burnup Program Written in FORTRAN-IV," Report LA-3671, Los Alamos Scientific Laboratory (in press).

7. "Liquid Metal Fast Breeder Reactor Design Study," Report WCAP-3251-1, Westinghouse (1964).

8. "Quarterly Status Report on the Advanced Plutonium Fuels Program October 1 - December 30, 1966," Report LA-3650-MS (1966).

9. D. P. Satkus and H. P. Flatt, "SIZZLE, a Fast or Intermediate Reactor Burnup Code," NAA Program Description, Code Number 58, Argonne Code Center, Argonne National Laboratory (1964).

PROJECT 812

TESTING AND EVALUATION OF NEUTRON CROSS SECTIONS FOR REACTOR CALCULATIONS

Person in Charge: D. B. Hall
Principal Investigator: G. H. Best

I. INTRODUCTION

For the evaluation of various fast breeder reactor concepts, good analytical techniques and cross sections are necessary. Valid comparisons between different concepts depend on minimization of differences in results due to methods of analysis. To this end, the Los Alamos Scientific Laboratory is cooperating with other AEC laboratories in the development of a uniform set of evaluated nuclear cross-section data and associated processing codes (ENDF/B). The Los Alamos Scientific Laboratory has prepared the data on ^{6}Li and ^{7}Li for the initial version of ENDF/B.

II. EVALUATION OF NUCLEAR DATA

(D. J. Dudziak, M. E. Battat, R. J. LaBauve)

The work of the Data Testing Subcommittee of the Cross Section Evaluation Working Group is divided into two phases of successive six-month periods. The Los Alamos Scientific Laboratory's participation will be as follows:

Phase I - November 1966 to May 1967

Review the ENDF/B data submitted for the following isotopes: ^{6}Li, ^{7}Li, ^{135}Xe, ^{176}Lu, ^{241}Am, and ^{243}Am. Make ENDF/B and associated codes (MC^2 and ETOE) operational at the Los Alamos Scientific Laboratory.

Phase II - May 1967 to November 1967

With ENDF/B and associated codes, generate multi-group cross sections for ZPR-III, Assembly No. 48. With the cross sections generated, calculate the following parameters:

Critical eigenvalue k

Relative fission ratios of materials involved

Reactivity worths of all materials specified

Neutron spectra and space-dependent fluxes

Doppler calculation at two temperatures specified

Reactivity change due to sodium voiding.

These calculations are to be compared with experiment and with calculations made with a standard Los Alamos Scientific Laboratory cross section set (Hansen-Roach).[1]

An early version of the MC^2 (multigroup constants) code was received from the Argonne National Laboratory and is now operational on the CDC-6600 computer. A more recent version of MC^2 is expected from the Brookhaven National Laboratory. This code is used in generating from the ENDF/B tape multigroup cross sections which are suitable for use in our reactor codes. Another code, ETOE, is being developed by the Atomic Power Development Associates for extracting desired data from ENDF/B and preparing it for MC^2 input.

Data and format requirements of ENDF/B for gamma-ray production (neutron-induced) and photon interactions are being investigated. Our participation in this area includes the determination of format requirements and recommendations on format and processing codes.

References

1. "Los Alamos Group-Averaged Cross Sections," L. D. Connolly, ed., Report LAMS-2941, Los Alamos Scientific Laboratory (1963).

PROJECT 814

EVALUATION OF CONTINUOUS MASS SPECTROMETRIC ANALYSIS OF SODIUM SYSTEM COVER GAS

Person in Charge: D. B. Hall
Principal Investigator: G. H. Best

I. INTRODUCTION

Cover gas analyzers for high-temperature sodium-cooled reactors must be capable of detecting impurities such as nitrogen, oxygen, hydrogen, carbon dioxide, and methane in the cover gas with a sensitivity adequate to measure impurities from the part per million range to the percent range. The analyses should be accurate to at least 5% and reproducible to about 1%.

Gas chromatographs are commonly used as gas analyzers for reactors. Conventional mass spectrometers are significantly more accurate for gas analysis of sodium cover gas. High temperature on-line operation will prevent adsorption of sodium compounds, fixed gases, and fission products on the walls of the apparatus.

II. HIGH TEMPERATURE RESIDUAL GAS ANALYZER
(N. G. Wilson and D. C. Kirkpatrick)

A. General

A wide range bakable quadrupole mass filter residual gas analyzer, which has recently become available commercially, can be operated at temperatures up to about 300°C. Work with high temperature sampling systems has indicated that the capability of the analyzer can probably be extended to temperatures of 500°-600°C. Special feedthrough devices in the analyzer assembly will allow on-line operation at that temperature. A field emission ion source will reduce fragmentation of molecules in the analyzer. A digital data handling system would allow real-time inspection of changes in the cover gas composition and on-line data reduction by a digital computer, which would be integrated into a general reactor monitoring and control system.

B. Current Results

A prototype analysis system has been constructed with which to investigate the special needs of 500°-600°C cover gas analysis apparatus. Design techniques used in the prototype are representative of those required for the 500°C-600°C system.

The prototype is now in operation and is exhibiting excellent performance. Initial tests have shown that the sampler-analyzer vacuum system is capable of producing 5×10^{-9} torr analyzer pressure with a 1×10^{-7} atm cc/sec sample rate into the analysis chamber from the sample chamber. Initial analysis of mass spectral data shows that it is possible to detect reliably partial pressures of approximately 10^{-14} torr in a total pressure of 10^{-8} torr.

Figures 1 and 2 show the compact arrangement of the apparatus. The gas handling system shown in Fig. 2 is behind the sampler-analyzer vacuum system instrumentation panels shown in Fig. 1 The sampler-analyzer vacuum system is fully automatic and is interlocked with the Electronic Associates Inc. QUAD 200 quadrupole analyzer.

Initial tests of a high speed core memory buffered analog-to-digital converter have been performed on the mass spectral data. The tests indicate that performing data analysis with this unit will give an order of magnitude improvement in effective detection sensitivity.

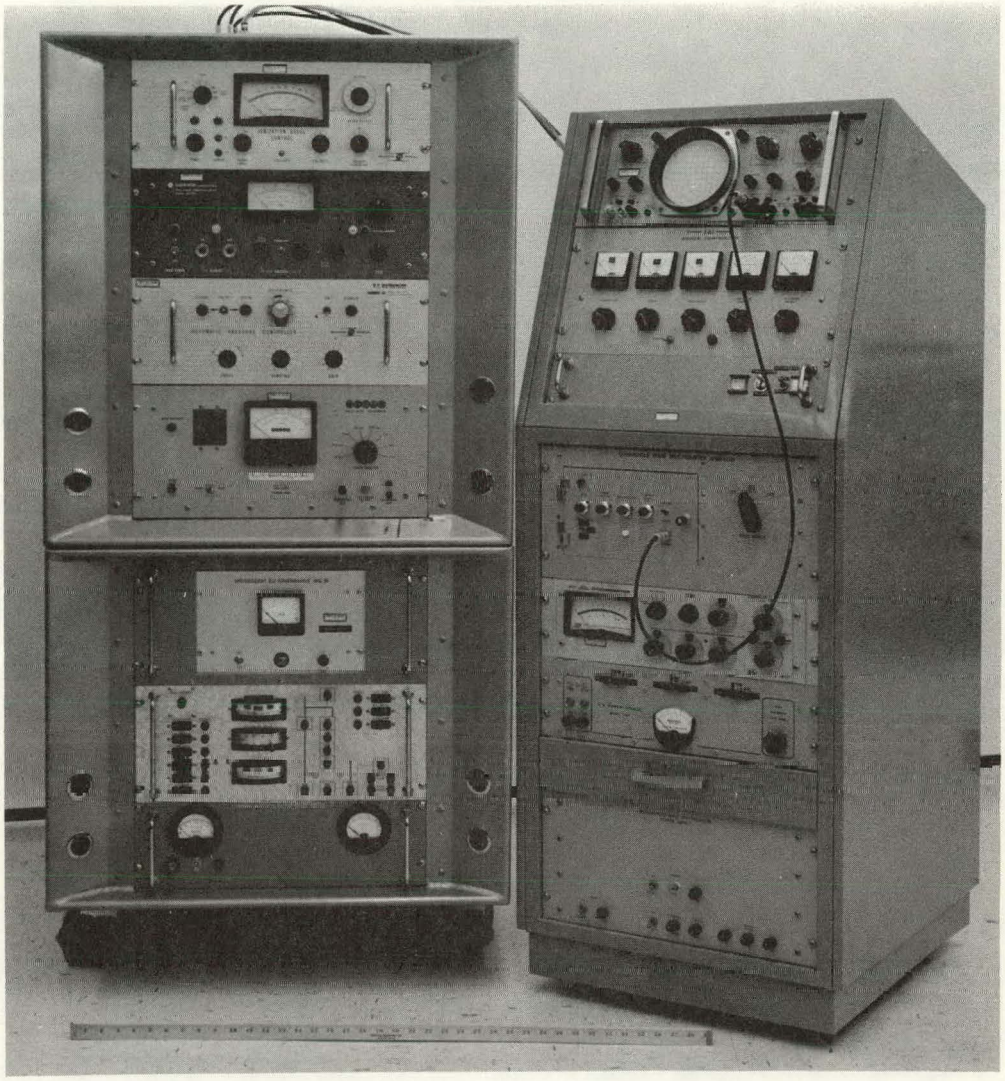

Fig. 1. Instrumentation panels for prototype high temperature cover gas analyzer system. This system will be used to investigate the special needs of a 500°-600°C cover gas analysis system. The analyzer will be capable of on-line analysis of cover gases in the 1 ppm range or lower. Sample rates from 10^{-7} atm cc/sec to 1 atm cc/sec can be accommodated. Initial tests of the prototype have shown sensitivities in the 0.1-1 ppm range.

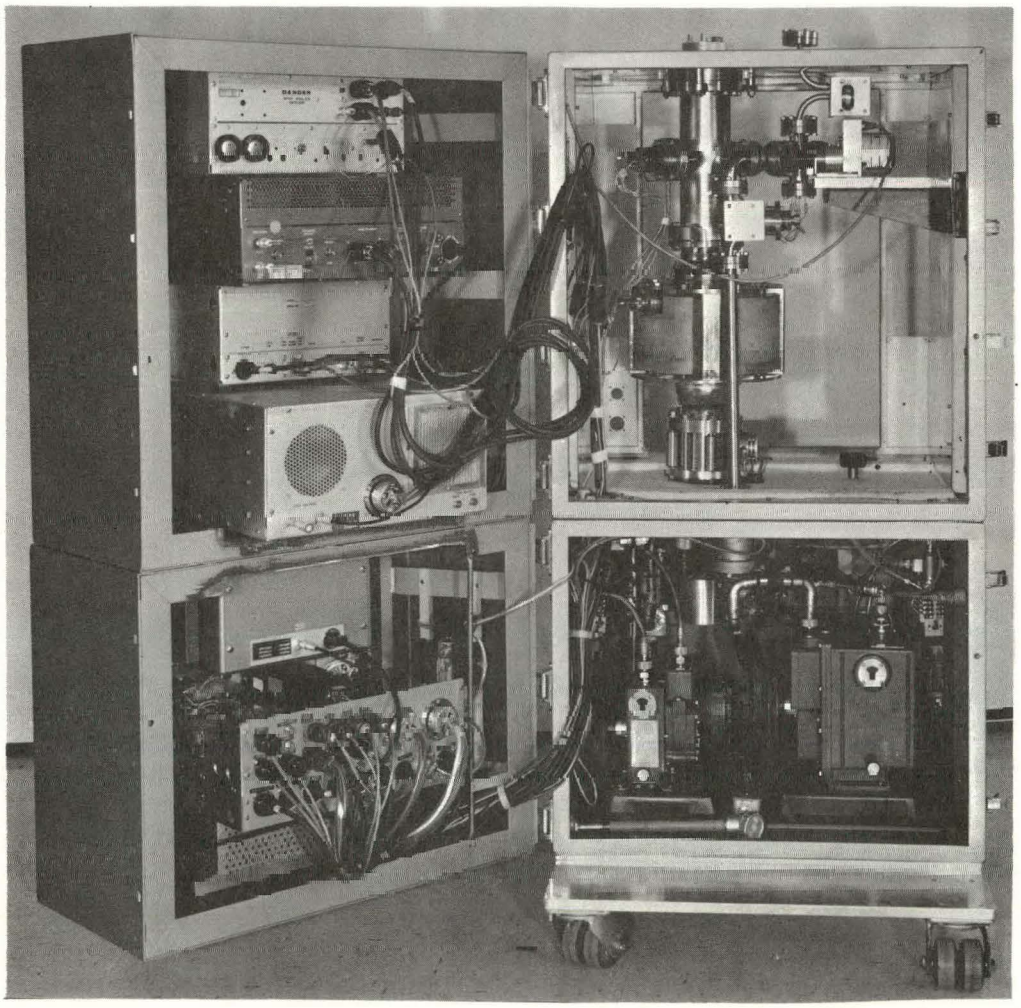

Fig. 2. Gas handling system for prototype high temperature cover gas analyzer system. This is a rear view of the apparatus shown in Fig. 1. Note the compact arrangement of the sampling vacuum system shown on the right side of the cabinet and the in-line stainless-steel analyzer vacuum chamber and pump system. The sampler-analyzer vacuum systems will be contained in an oven chamber in the upper cabinet to give an operating system temperature of 250°C.

PROJECT 816

ADVANCED MEASUREMENT AND ANALYSIS TECHNOLOGY

Person in Charge: D. B. Hall
Principal Investigator: G. H. Best

I. INTRODUCTION

The purpose of this project is to define, develop, and demonstrate advanced instrumental measurement and analysis techniques for the liquid-metal-cooled fast reactor program. Current activity on this project is concentrated on three tasks; the measurement of gaseous diffusion rates in metals, the correlation of nondestructive tests with liquid metal coolant leaks, and the development of gamma-ray scanning techniques for reactor applications.

II. MEASUREMENT OF GASEOUS DIFFUSION RATES IN METALS
(N. G. Wilson)

A. General

Very little quantitative information is available on the diffusion of gases in containment materials for reactor systems, although this phenomenon is known to occur in high-temperature liquid-metal-cooled systems. By use of ultra-high vacuum techniques and a mass spectrometer residual gas analyzer, diffusion rates of 10^{-11} to 10^{-12} torr-liter/sec-cm^2 ($\approx 10^{-13}$ to 10^{-14} g/sec) equivalent nitrogen should be easily observable by a pressure drop across a geometrically fixed impedance. Gases of molecular weight up to 500 and metals of interest to the LMFBR and FFTF projects will be studied.

B. Current Results

An apparatus to test a new method of flow measurement in ultra-high vacuum is being constructed. The flow measurement technique will use a distributed orifice (electroformed nickel mesh) in conjunction with two (or more) axially mounted nude hot cathode ionization gauges. With this arrangement, it should be possible to measure accurately the gas flow rate through a metering section between the diffusion test cell and the vacuum pump.

An experimental apparatus with which to perform the various measurements is being designed. With this apparatus, it will be possible to measure diffusion through a metal from a gas as well as diffusion of dissolved gases from sodium through a metal. Analysis of sodium cover gas and gases that have diffused through the metal sample will be possible. In order to provide an environement like that of a reactor coolant system, a dynamic sodium system will be used.

III. CORRELATION OF NONDESTRUCTIVE TEST WITH LIQUID METAL COOLANT LEAKS
(N. G. Wilson and D. C. Kirkpatrick)

A. General

Helium mass spectrometer leak detection is customarily used as a quality control method during fabrication of sodium-containing reactor coolant systems. It is usually specified that such systems should show no leaks in excess of 10^{-7} to 10^{-8} standard cc/sec helium, although experience at the Los Alamos Scientific Laboratory has shown that for loop temperatures above 500°C, an unreparable helium leak of about 10^{-9} standard cc/sec will probably result in a sodium leak within the first year of operation. By studying mechanisms and characteristics of helium molecular transport rates through microscopic penetrations in metals, we hope to correlate helium leak rates with those of liquid metal coolants.

This study will use fabricated stainless steel leaks with a range of helium leak rates. Each of these leaks will be incorporated into a small sodium

system which will be held at a predetermined temperature until sodium leakage occurs.

B. Current Results

A furnace support rack designed to accommodate eight groups of four test furnaces has been completed. This rack is arranged so that each module of four furnaces is isolated from all other modules, provided with its own air-sweep system, and supplied by its own power supply and instrumentation cabling. The air-sweep system is designed so that sodium leak detection instrumentation can easily be evaluated on this apparatus. Four furnaces have been installed in one module of the furnace support rack.

A reference design has been developed for a sodium test cell to be used in the furnaces. This design will allow vacuum outgassing of the test cell as well as sodium filling without exposure to the atmosphere. Four test cells are being fabricated in order to evaluate the design and handling procedures.

Initial tests of a leak fabrication apparatus (Fig. 1) are in progress. This apparatus will use an ultra-high vacuum environment and high pressure, cold diffusion of metal to produce stable leak paths in stainless steel. Initial tests with >200,000 psi loading under ambient pressure produced usable leaks of from 10^{-5} to 10^{-8} atm cc/sec helium. It was not possible, however, to predict the size of the leak

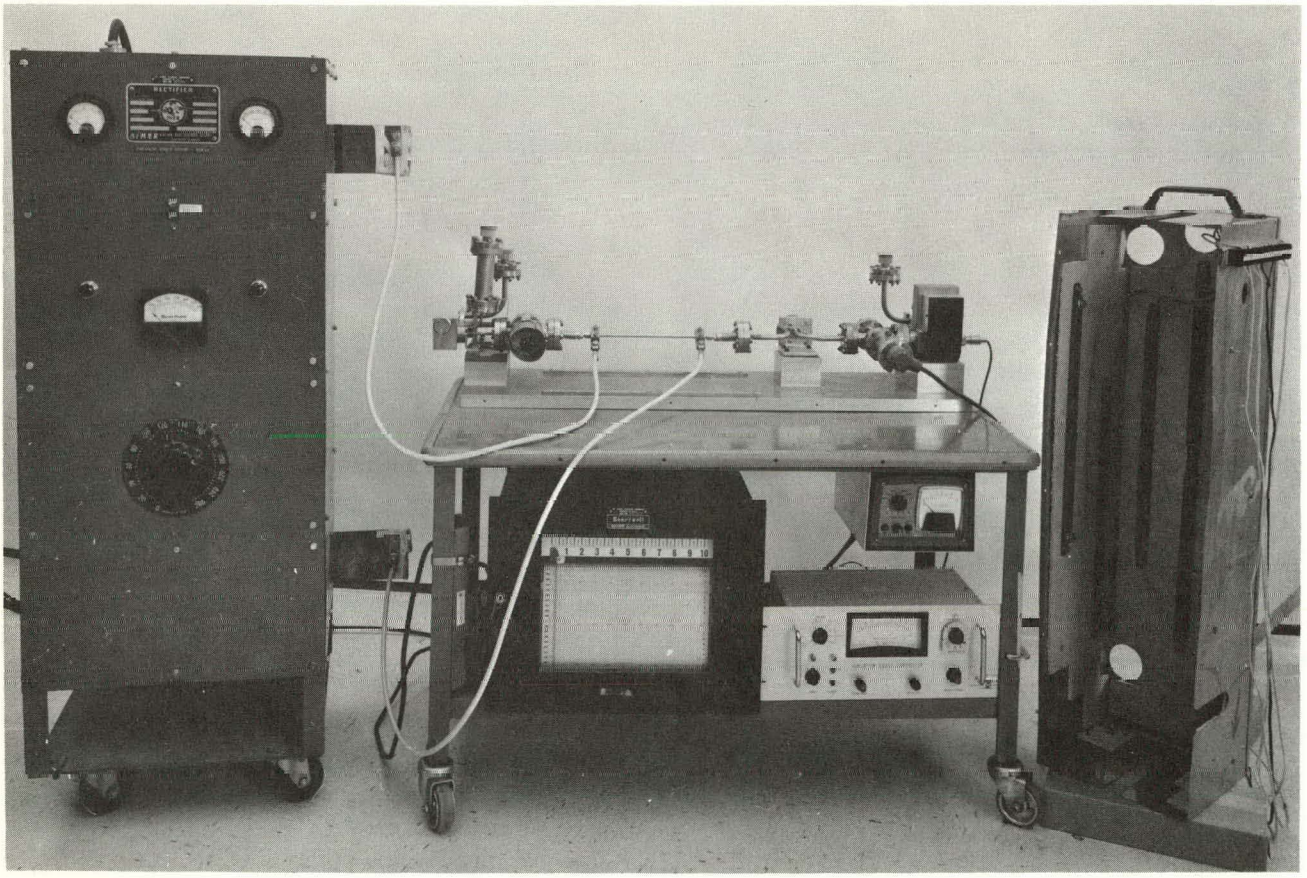

Fig. 1. Leak fabrication apparatus for investigation of leaks in sodium systems. Leaks will be fabricated in this apparatus by (a) evacuating the tube from which the leak will be formed to a pressure of approximately 1 x 10^{-9} torr, (b) heating the tube electrically to a temperature of 400°-500°C, and (c) collapsing the tube, still at ultra high vacuum (<1 x 10^{-8} torr) in a 30-ton hydraulic press. Cold welding of most of the tube wall is expected to produce a thermally stable leak.

from fabrication data. The use of ultra-high vacuum should allow reproducible fabrication.

IV. GAMMA SCANNING TECHNIQUES
(D. M. Holm)

A. General

Studies of fission product concentrations and distributions in irradiated fuel and blanket materials can yield information not readily obtainable by other means. For example, the relative abundances of certain gaseous fission products in a fuel element can be used to assess the integrity of the fuel cladding. In many applications of gamma scanning it is important to have detectors with good energy resolution and background discrimination. More detailed information is then available from the data, provided it can be recorded and analyzed in a reasonable period of time. The improvement of detectors, and the development of automated data acquisition and reduction schemes, therefore, form large parts of this work.

B. Current Results

1. Equipment

Temperature control of the gamma-scanning instrumentation is necessary for analyzer stability. To solve this problem, an air-conditioned semitrailer has been obtained, and the instruments are being installed in it. This trailer will also provide the necessary degree of mobility for off-site experiments.

2. Computer Predicition of Gamma-Ray Spectra

In order to interpret gamma spectra from reactor fuels irradiated in a fast-neutron flux, elaborate analysis of the data is required. A FORTRAN-IV code has been written which uses existing data on gamma decay to predict what the spectra from a neutron-irradiated material should be as a function of time. At present, the major limitations of the code are the uncertainties of the fission product yields for fast fission of plutonium and the uncertainties of decay schemes.

In order to obtain information on the fission product yields for fast fission of plutonium, plutonium samples will be irradiated with fast neutrons from Jezebel, a Los Alamos fast critical assembly, and gamma-ray spectra from the irradiated samples will be observed and analyzed. Twenty samples, from which gamma-ray spectra will be observed above 300 keV, will be 0.394 in. in diameter by 34 mils thick, and 10 samples will be 0.394 in. in diameter by 4 mils thick; making use of the thinner samples will make it possible to observe gamma-ray spectra at energies below 100 keV. The samples will be canned in 5-mil-thick nickel. Calculations indicate that the nickel will cause negligible background counts.

SPECIAL DISTRIBUTION

Atomic Energy Commission, Washington

Division of Research

D. K. Stevens

Division of Naval Reactors

R. H. Steele

Division of Reactor Development and Technology

Lewis J. Colby
G. W. Cunningham
Donald E. Erb
Nicholas Grossman
Kenneth E. Horton
DeWitt Moss
R. E. Pahler
J. M. Simmons (2)
Edward E. Sinclair
A. Van Echo
G. W. Wensch
M. J. Whitman
I. F. Zartman (2)

Division of Space Nuclear Systems

G. K. Dicker
F. C. Schwenk

Ames Laboratory, ISU

O. N. Carlson
W. L. Larsen
M. Smutz

Argonne National Laboratory

Alfred Amorosi
Frank G. Foote
J. H. Kittel
R. E. Machorcy
M. V. Nevitt

Atomics International

C. E. Weber

Babcock & Wilcox Co.

C. Baroch
J. H. MacMillan

Battelle Memorial Institute

D. Keller
S. Paprocki

Brookhaven National Laboratory

D. H. Gurinsky
C. Klamut

Combustion Engineering, Inc.

S. Christopher

General Atomics

D. Ragone

General Electric Co., Cincinnati

V. P. Calkins

General Electric Co., Pleasanton

E. A. Evans
A. N. Holden

General Electric Co., KAPL

W. Cashin

Idaho Nuclear

W. C. Francis

IIT Research Institute

R. Van Tyne

Lawrence Radiation Laboratory

Leo Brewer
J. S. Kane
A. J. Rothman

Mound Laboratory

R. G. Grove

NASA, Lewis Research Center

J. J. Lambardo

Naval Research Laboratory

L. E. Steele

Oak Ridge National Laboratory

G. M. Adamson
J. E. Cunningham
J. H. Frye, Jr.
C. J. McHargue
P. Patriarca
O. Sisman
M. S. Wechsler
J. R. Weir

Pacific Northwest Laboratory

F. W. Albaugh
E. R. Astley
J. M. Davidson

Bureau of Mines, Albany, Oregon

H. Kato

United Nuclear Corp.

A. Strasser

Westinghouse Atomic Power Division

W. E. Ray

Westinghouse, Bettis Atomic Power Laboratory

E. J. Kreigh